Genetic Dissection of Peroxisome-Associated Matrix Protein Degradation in *Arabidopsis thaliana*

Sarah E. Burkhart, Matthew J. Lingard,[1] and Bonnie Bartel[2]
Department of Biochemistry and Cell Biology, Rice University, Houston, Texas 77005

ABSTRACT Peroxisomes are organelles that sequester certain metabolic pathways; many of these pathways generate H_2O_2, which can damage proteins. However, little is known about how damaged or obsolete peroxisomal proteins are degraded. We exploit developmentally timed peroxisomal content remodeling in *Arabidopsis thaliana* to elucidate peroxisome-associated protein degradation. Isocitrate lyase (ICL) is a peroxisomal glyoxylate cycle enzyme necessary for early seedling development. A few days after germination, photosynthesis begins and ICL is degraded. We previously found that ICL is stabilized when a peroxisome-associated ubiquitin-conjugating enzyme and its membrane anchor are both mutated, suggesting that matrix proteins might exit the peroxisome for ubiquitin-dependent cytosolic degradation. To identify additional components needed for peroxisome-associated matrix protein degradation, we mutagenized a line expressing GFP–ICL, which is degraded similarly to endogenous ICL, and identified ***p****ersistent GFP-ICL* ***fl****uorescence* (*pfl*) mutants. We found three *pfl* mutants that were defective in *PEROXIN14* (*PEX14/At5g62810*), which encodes a peroxisomal membrane protein that assists in importing proteins into the peroxisome matrix, indicating that proteins must enter the peroxisome for efficient degradation. One *pfl* mutant was missing the peroxisomal 3-ketoacyl-CoA thiolase encoded by the *PEROXISOME DEFECTIVE1* (*PED1/At2g33150*) gene, suggesting that peroxisomal metabolism influences the rate of matrix protein degradation. Finally, one *pfl* mutant that displayed normal matrix protein import carried a novel lesion in *PEROXIN6* (*PEX6/At1g03000*), which encodes a peroxisome-tethered ATPase that is involved in recycling matrix protein receptors back to the cytosol. The isolation of *pex6-2* as a *pfl* mutant supports the hypothesis that matrix proteins can exit the peroxisome for cytosolic degradation.

PEROXISOMES are single-membrane-bound organelles that house essential metabolic pathways in plants and other eukaryotes. For example, peroxisome biogenesis defects underlie the Zellweger spectrum of human congenital disorders, which often are fatal in infancy (reviewed in Wanders and Waterham 2005). Similarly, peroxisomes are essential for plant embryogenesis and development following germination (reviewed in Hu *et al.* 2012). The essential role of plant peroxisomes likely reflects the importance of peroxisomal enzymes, which catalyze key steps in photorespiration, fatty acid β-oxidation, jasmonate production, and conversion of the protoauxin indole-3-butyric acid (IBA) to the active auxin indole-3-acetic acid (IAA) (reviewed in Hu *et al.* 2012).

Peroxisomes import matrix proteins from the cytosol with the assistance of peroxin (PEX) proteins. Most matrix proteins are directed to the peroxisome by a C-terminal peroxisome-targeting signal 1 (PTS1) that binds the cytosolic receptor PEX5 (Keller *et al.* 1987). PEX5-cargo complexes dock with the PEX13 and PEX14 membrane peroxins (reviewed in Azevedo and Schliebs 2006; Williams and Distel 2006) at the peroxisome membrane. Other matrix proteins use an N-terminal PTS2 to bind the cytosolic receptor PEX7 (Osumi *et al.* 1991; Swinkels *et al.* 1991). In plants and mammals, PEX7 depends on PEX5 (Matsumura *et al.* 2000; Hayashi *et al.* 2005; Woodward and Bartel 2005) for cargo delivery to the PEX13 and PEX14 docking peroxins (reviewed in Lazarow 2006). After matrix proteins are delivered, yeast PEX5 is ubiquitinated in the peroxisome membrane by the ubiquitin-conjugating enzyme PEX4 and the ubiquitin-protein ligase PEX12 (Platta *et al.* 2009). Ubiquitinated PEX5 is retrotranslocated to the cytosol with the assistance of the peroxisome-tethered ATPases PEX1 and PEX6 (reviewed in Fujiki *et al.* 2012; Grimm *et al.* 2012) to be reused in further rounds of import.

Many metabolic pathways sequestered in peroxisomes produce hydrogen peroxide (H_2O_2). For example, H_2O_2 is

Copyright © 2013 by the Genetics Society of America
doi: 10.1534/genetics.112.146100
Manuscript received September 24, 2012; accepted for publication November 1, 2012
[1]Present address: 700 Chesterfield Parkway, Chesterfield, MO 63017.
[2]Corresponding author: Department of Biochemistry and Cell Biology, MS-140, Rice University, 6100 Main St., Houston, TX 77005. E-mail: bartel@rice.edu

generated by the acyl-CoA oxidases acting in fatty acid β-oxidation (Eastmond *et al.* 2000b; Adham *et al.* 2005) and the glycolate oxidases acting in photorespiration (Fahnenstich *et al.* 2008). H_2O_2 can damage proteins (Van Den Bosch *et al.* 1992; Willekens *et al.* 1997), but little is known about how damaged or obsolete peroxisomal proteins are degraded. Three possible mechanisms for peroxisomal matrix protein degradation can be envisioned: degradation within the organelle by resident proteases, degradation of the entire organelle via autophagy, or retrotranslocation out of the organelle followed by cytosolic degradation.

Many organelles, including mitochondria and chloroplasts, contain proteases that degrade damaged or misfolded proteins (reviewed in Leidhold and Voos 2007). Several proteases are found in *Arabidopsis* peroxisomes (Reumann *et al.* 2004, 2007; Helm *et al.* 2007; Lingard and Bartel 2009). For example, DEG15 cleaves PTS2 proteins from their targeting signal after import (Helm *et al.* 2007; Schumann *et al.* 2008) and the LON2 ATP-dependent protease is needed for sustained matrix protein import (Lingard and Bartel 2009). Although a fungal LON isoform contributes to degradation of oxidatively damaged peroxisomal matrix proteins (Bartoszewska *et al.* 2012), no resident peroxisomal proteases have been implicated in matrix protein degradation in plants.

A second possibility for peroxisomal protein degradation is removal of the entire organelle by autophagy or pexophagy, a specialized form of autophagy. For example, yeast use pexophagy to degrade excess peroxisomes by encasing the peroxisome in a membrane for fusion with the vacuole (reviewed in Manjithaya *et al.* 2010). Although autophagy occurs in *Arabidopsis* (reviewed in Li and Vierstra 2012), pexophagy has not been reported in plants.

A third potential mechanism for peroxisome-associated protein degradation is modeled after ER-associated protein degradation (ERAD), the process by which misfolded proteins are ubiquitinated and retrotranslocated from the ER lumen to the cytosol for proteasomal degradation (reviewed in Hoseki *et al.* 2010). Peroxins needed for PEX5 ubiquitination and retrotranslocation resemble ERAD components (Gabaldon *et al.* 2006; Schluter *et al.* 2006), suggesting that damaged peroxisomal proteins may be retrotranslocated out of the peroxisome and degraded in the cytosol by the 26S proteasome (Zolman *et al.* 2005).

Some evidence in *Arabidopsis* is consistent with a retrotranslocation model for matrix protein degradation. Isocitrate lyase (ICL) and malate synthase (MLS) are peroxisomal glyoxylate cycle enzymes that enable carbon from acetyl-CoA to be utilized in gluconeogenesis, thus providing energy for germinating seedlings (reviewed in Graham 2008). In *Arabidopsis*, ICL and MLS are degraded a few days after germination (Zolman *et al.* 2005; Lingard *et al.* 2009). Mutation of the PEX4 ubiquitin-conjugating enzyme along with PEX22, which tethers PEX4 to the peroxisome (*pex4-1 pex22-1*; Zolman *et al.* 2005), partially stabilizes MLS, ICL, and a GFP–ICL translational fusion without markedly impairing matrix protein import (Zolman *et al.* 2005; Lingard *et al.* 2009). Stabilization of these glyoxylate cycle enzymes in *pex4-1 pex22-1* suggests a role for PEX4-mediated ubiquitination in promoting matrix protein degradation.

To identify additional components necessary for the turnover of damaged or unnecessary peroxisomal proteins, we initiated a forward genetic screen for *Arabidopsis* mutants exhibiting delayed GFP–ICL degradation. We identified several mutants with prolonged GFP–ICL fluorescence that also stabilized endogenous ICL. Characterization of these mutants confirmed that matrix proteins must enter the peroxisome to be subject to efficient degradation and is consistent with the possibility that damaged or obsolete matrix proteins can exit the peroxisome for cytosolic degradation.

Materials and Methods

Plant materials and growth conditions

Arabidopsis thaliana accession Columbia (Col-0) or Col-0 transformed with *ICLp:GFP–ICL*, which drives a GFP–ICL fusion protein from the *ICL* 5′-regulatory region (Lingard *et al.* 2009), was used as wild type (as indicated in figure legends). *pex14-1*, *pex14-2*/SALK_007441, *pex14-3*/SALK_072373, *pex14-4* (Monroe-Augustus *et al.* 2011), *ped1-96* (Lingard and Bartel 2009), *lon2-2*/SALK_043857 (Lingard and Bartel 2009), *pex6-1* (Zolman and Bartel 2004), and *pex6-1* lines transformed with *pBINPEX6*, *35S:HsPEX6*, and *35S:PEX5* (Zolman and Bartel 2004) were previously described. Prior to phenotypic analyses, *pfl7/ped1-7*, *pfl20/lon2-6*, *pfl47/pex6-2*, *pfl49/pex14-6*, and *pfl175/pex14-5* were backcrossed to wild-type Col-0 at least once. Unidentified mutants (*pfl29*, *pfl99*, and *pfl106*) and the second *pex14-5* isolate (*pfl164)* were characterized using nonbackcrossed progeny of original isolates. *pex6-2* carrying *pBINPEX6*, *35S:HsPEX6*, or *35S:PEX5* were generated by *Agrobacterium tumefaciens*-mediated transformation (Clough and Bent 1998) of backcrossed *pex6-2* lacking the *ICLp:GFP-ICL* transgene. Homozygous lines were selected in the progeny of transformants by following resistance to kanamycin (*pBINPEX6*) or glufosinate ammonium (Basta) (*35S:HsPEX6* and *35S:PEX5*).

Surface-sterilized seeds were plated on plant nutrient (PN) medium (Haughn and Somerville 1986) supplemented with 0.5% (w/v) sucrose (PNS) and solidified with 0.6% (w/v) agar. Hormone stocks were dissolved in ethanol at 10 or 100 mM and media normalized to the same ethanol content were used as controls. For assays of light-grown seedlings, seeds were stratified for 1 day, plated on the indicated auxin concentrations, and grown for 8 days at 22° under continuous illumination through yellow long-pass filters, which slow indolic compound breakdown (Stasinopoulos and Hangarter 1990), unless otherwise indicated. For assays with dark-grown seedlings, seeds were stratified for 1 day, allowed to begin germination in the absence of hormones under yellow light for 1 day, plated on the indicated media, returned to yellow light for 1 day, and placed in darkness for 4 or 5 days, after which hypocotyl lengths were measured.

Table 1 Markers used in recombination mapping

Marker	Nearest gene	Enzyme	Fragment size (bp) Col-0	Fragment size (bp) L*er*	Primer sequences (or reference)
nga63	*At1g09920*	—	111	89	Bell and Ecker (1994)
MAR109	*At1g17290*	*Bsa*BI	597	353, 244	TTTTTGGGGGTTCTCAGGTTATC GCACGCTCAATCGAATCAGAAC
LCS1114	*At1g28500*	*Dde*I	231, 207	438	AGAAAATGAGAAGCCCCTGGATAAG CGCGGCTCTGTTCTTGATGTTTC
SEC202	*At2g41230*	*Hpa*I	413	296, 117	TGAATTATGACGCAGCTGGAAGAAAAGAGAC TAAAGAGGCGTAAATAGAATGAGG
SEC242	*At2g46250*	*Taq*I	112	85, 27	GGACTTCAGCCCATGTATTCACCT CGTCAACGGATCACCTCAACCTA
SEC321	*At3g07810*	*Rsa*I	137, 29	166	AAAAACAATAAAGATGCAGAATGGCTACT TTTGATTATCCTCGTCTTCTTTCTGGAATG
F24K9	*At3g11590*	*Bgl*II	200, 30	230	AATTTAAAATTATATGCAAACTAATTAGAT GTAGCTAAAAAGTTGCTGCAAGCAAGGAAA
SO191	*At5g37780*	—	180	200	Copenhaver *et al.* (1998)
ILL3	*At5g54140*	*Nde*I	360	260, 100	Davies *et al.* (1999)

For lateral root assays, seeds were stratified for 1 day, plated on PNS, and grown in yellow light for 4 days. Four-day-old seedlings were then transferred to a mock or IBA-containing PNS plate and grown under yellow light for 4 additional days, after which the primary root length was measured and the number of lateral roots that had emerged from the primary root were counted.

Mutant isolation and recombination mapping

Seeds from Col-0 lines transformed with *ICLp:GFP-ICL* (Lingard *et al.* 2009) were mutagenized with ethyl methanesulfonate (EMS; Normanly *et al.* 1997). M_2 seeds were surface sterilized (Last and Fink 1988), stratified for 0–1 day, plated on PNS (~1000 seeds per 100 × 100 × 15 mm square plate), and grown in white light. Mutants displaying GFP–ICL fluorescence at 7–9 days were selected using a Leica MZ FLIII fluorescence stereomicroscope equipped for GFP detection, transferred to a fresh PNS plate to recover, and moved to soil for seed production. For retesting, M_3 progeny seeds were stratified for 3 days to promote uniform germination and assayed for prolonged fluorescence after 6–7 days of growth under white light. Lines displaying prolonged fluorescence were retained as ***p**ersistent GFP-ICL **fl**uorescence (pfl)* mutants.

Mutants isolated from Col-0 carrying the *ICLp:GFP-ICL* construct were outcrossed to Landsberg *erecta* (L*er*) for recombination mapping. F_2 seedlings from *pfl47* and *pfl106* outcrosses were screened on PNS for prolonged GFP–ICL fluorescence compared to the unmutagenized parent lines and F_3 progeny of mapping plants were confirmed to have prolonged fluorescence. F_2 seedlings from *pfl7* and *pfl99* outcrosses were screened for sucrose dependence. F_2 seedlings from *pfl20* and *pfl29* outcrosses were screened for IBA-resistant root elongation. DNA was isolated from individuals in the mapping populations showing the mutant phenotype and assayed using published and newly developed PCR-based polymorphic markers (Table 1).

Immunoblot analysis

To avoid complications in assessing the timing of ICL or MLS degradation that would arise if a mutant exhibited delayed germination, time-course immunoblots used seedlings that had germinated within 24 hr after plating. Protein was extracted from seedlings grown under continuous white light on PNS for the indicated number of days. To extract protein, frozen tissue was ground with a pestle and two volumes of 2× loading buffer (Invitrogen, Carlsbad, CA) was added. Samples were centrifuged and 20 μl of supernatant was transferred to a fresh tube with 2.1 μl of 0.5 M dithiothreitol and heated at 100° for 5 min. Samples were loaded onto NuPAGE 10% Bis-Tris gels (Invitrogen) next to prestained protein markers (P7708S, New England Biolabs, Beverly, MA) and Cruz Markers (Santa Cruz Biotechnology, Santa Cruz, CA). After electrophoresis, proteins were transferred for 30 min at 24 V to a Hybond ECL nitrocellulose membrane (Amersham Pharmacia Biotech, Piscataway, NJ) using NuPAGE transfer buffer (Invitrogen). After transfer, membranes were rocked for 1 hr at 4° in blocking buffer (8% nonfat dry milk, 20 mM Tris, pH 7.5, 150 mM NaCl, 0.1% Tween-20) and incubated overnight at 4° with primary antibodies diluted in blocking buffer: rabbit α-GFP (1:300 dilution, BD Biosciences 8372-2), rabbit α-ICL (1:2,000 dilution, Maeshima *et al.* 1988), rabbit α-HPR (1:1000 dilution, Agrisera AS11 1797 or Kleczkowski and Randall 1988), rabbit α-MLS (1:25,000 dilution; Olsen *et al.* 1993), rabbit α-PEX5 (1:100 dilution; Zolman and Bartel 2004), rabbit α-PEX6 (1:1,000 dilution; Ratzel *et al.* 2011), rabbit α-PEX7 (1:800 dilution; Ramón and Bartel 2010), rabbit α-PEX14 (1:2,500 dilution, Agrisera AS08 372), rabbit α-PMDH2 (1:2,000 dilution; Pracharoenwattana *et al.* 2007), rabbit α-thiolase (PED1 isoform, 1:10,000 dilution; Lingard *et al.* 2009), or mouse α-HSC70 (1:20,000–1:30,000 dilution, StressGen Bioreagents SPA-817), followed by a 4-hr incubation with horseradish peroxidase-linked goat

Table 2 Primers used for amplification and sequencing of candidate genes

Gene/accession no.	Primer names	Primer sequences
PEX14/At5g62810	PED2-1 and	CATCCTCATCATCTCTCATCAT
	PED2-2	CTTAATGGCCTAACCATTTTATCCCAC
	PED2-3 and	GGGTTACTTGGCATAGTCCTCTAAAGACG
	PED2-4	GGACGTGTGTCATAATCAACATTGCTG
	PED2-5 and	GGTAACATTAGGAACCTTGATATGTGATGC
	PED2-6	GGCAAACCTCATAAAGTATCAATAACCCG
PED1/At2g33150	PED1-11 and	TTCCCGCACATTCTGATGATGACC
	PED1-12	AGAAATGGCTGCCACCCAAA
	PED1-13 and	GACATAGGCATTGATAGAGAAGACGAATCT
	PED1-8	AAGTACCAGCAGTAGTGGTGCCAT
	PED1-14 and	TGTTGACCCGAAGACTGGTGATGAGAAAC
	PED1-15	AGATATATCTCGGCTGTGGATTTCTTAAGG
	PED1-16 and	ATCTGGGCTTCAGGCTGTTGCTGAT
	PED1-17	TGCCTTTCTGTGCGAGTCAACCTA
LON2/At5g47040	LON2-1s and	CTCATAAGTGTTGCCTTTCGCTAAATCCC
	LON2-2s	CCACATTCACTTTCCTGCTGG
	LON2-3s and	CTTATCTTTGATGCCACCAACAGGCAGAAC
	LON2-4s	GTCTGTATTGACTGTTACCCTTAACGG
	LON2-5s and	CAGATGGCGCATAGCTATCTTAAG
	LON2-6s	GATGGTGTGTGACTGTGGACCAACTTG
	LON2-7s and	GGCTAAACCATAGTGATCACTGTCAAGACG
	LON2-8s	TAGTTTCGACTTAGAGCTTATTTGG
	LON2-9s and	CTGGATCTTGTTTTACTTGCTCCAACTc
	LON2-10s	GAAACAGTGGAGCTCCCGAGTAGGTTAGCG
	LON2-11s and	GATCGAAGCGTAAGAATGTTAGGAATTGAG
	LON2-12s	GTAATGTAATGGGCCTTAGTCTCATTGTTTC
PEX6/At1g03000	PEX6-7 and	ATCCTCTTCAGTCTTCATCGGTTCG
	PEX6-8	CGATGTACGAGGGATTTCAGGCAAGATA
	PEX6-9 and	ACTCTGGTTCTTTGGTATGTCCTTCTC
	PEX6-10	CTAAATTCAACTACATGCAGCCCCAACCTC
	PEX6-11 and	CCAGGTACATTTGCTTCGGTTTC
	PEX6-12	GCGATTAGCAGCACTTGATGTCC
	PEX6-13 and	GATTTTCATTTCTTTCCTTGGTTCTC
	PEX6-14	AATGGCTTACTTACTTTCCCTGTTCC
	PEX6-15 and	AAATGTGAAATGGGATGATGTTGGTG
	PEX6-16	AAACACAAACCTAATATAACAAACTGATGAT

α-rabbit or α-mouse IgG secondary antibody (1:5000 dilution in blocking buffer, Santa Cruz Biotechnology, SC2030 or SC-2031). Horseradish peroxidase was visualized by incubation with LumiGlo reagent (Cell Signaling Technology, Danvers, MA) or WesternBright ECL reagent (Advansta, Menlo Park, CA).

RNA analysis

RNA was isolated from 8-day-old light-grown Col-0 and *pex14-6* seedlings using the TRI Reagent RNA Extraction method according to the instructions of the manufacturer (Sigma, St. Louis, MO) and dissolved in DEPC-treated water. cDNA was synthesized from RNA using a 3′ gene-specific primer (PED2-6; Table 2) and SuperScript III reverse transcriptase (Invitrogen, Carlsbad, CA). The *pex14-6* cDNA was PCR amplified across the exon 1–2 junction using PED2-1 and PED2-4 primers (Table 2) and sequenced using PED2-1.

Confocal microscopy

Four-day-old seedlings carrying *ICLp:GFP-ICL* (Lingard *et al.* 2009) were mounted in water under a cover glass. Images were collected using a Carl Zeiss LSM 710 laser scanning confocal microscope equipped with a Meta detector. Samples were imaged through a 40× oil immersion objective after excitation with a 488-nm argon laser; GFP emission was collected between 494 and 560 nm. Each image is an average of 8 exposures using a 70-μm pinhole, corresponding to a 1.8-μm optical slice.

Sequencing and genotyping of mutant lesions

Candidate genes in mapping intervals were PCR amplified from mutant genomic DNA using primers listed in Table 2. Amplicons were purified using Zymo PCR purification kit (Zymo Research, Irvine, CA) and sequenced directly (Lone Star Labs, Houston, TX) with the primers used for amplification.

The *PEX14* gene (*At5g62810*) was amplified from *pfl49*, *pf164*, and *pf175* genomic DNA using three oligonucleotide pairs (Table 2). The resulting overlapping fragments covered the gene from 75 bp upstream of the translation start site to 29 bp downstream of the stop codon. The lesion identified in *pfl49* changed *PEX14* G73 (where 1 is the first nucleotide of the initiator codon) to an A, which altered a splice site. The lesion identified in *pfl164* and *pfl175*

Table 3 PCR-based markers for determining genotypes of identified mutations

Mutant	Primer names	Primer sequences	Enzyme	Product size (bp)	
				Wt	Mutant
pfl7/ped1-7	PED1-7	GAAATTCCAGCCAAGTAAGTGATG	*Dpn*II	125	100, 25
	PED1–*Dpn*II[a]	CGTAGCTTTGTAAGTAATTATTACCGA			
pfl20/lon2-6	LON2-14	AATTTGTTCGCTTATCTTTGGGTGGTGT	*Mln*I	57, 42	99
	LON2-15	CTCCCCAAGTTCCTCATCAGCATAAGC			
pfl47/pex6-2	PEX6-19	AGGAACCTTTGATCTATACACCAGT	*Ava*II	62, 29	91
	PEX6–*Ava*II[a]	AGTGAATCACTCCCAAACCGCCCTGGTC			
pfl49/pex14-6	PED2-1	CATCCTCATCATCTCTCATCAT	*Ava*II	150, 30	180
	PED2–*Ava*II[a]	GAAATAATGATTAGAAGGTGTAAATTGGAC			
pfl164/175/ pex14-5	PED2-2	CATCCTCATCATCTCTCATCAT	*Rsa*I	156, 25	181
	PED2–*Rsa*I	GACTGGGAGGTAATTTTGTATG			

[a] This is a dCAPS oligonucleotide (Michaels and Amasino 1998; Neff *et al.* 1998); the underlined nucleotide differs from wild-type sequence to create a restriction site in either the mutant or wild-type PCR amplicon.

(which are likely siblings as they were isolated from the same pool of mutagenized seeds) changed *PEX14* G904 (where 1 is the first nucleotide of the initiator codon) to an A, which changed Trp152 to a stop codon.

The *PED1* gene (*At2g33150*) was amplified from *pfl7* genomic DNA using four oligonucleotide pairs (Table 2). The resulting overlapping fragments covered the gene from 72 bp upstream of the translation start site to 274 bp downstream of the stop codon. The lesion identified in *pfl7* changed G2624 (where 1 is the first nucleotide of the initiator codon) of *PED1* to an A, which altered a splice site.

The *LON2* gene (*At5g47040*) was amplified from *pfl20* genomic DNA using six oligonucleotide pairs (Table 2). The resulting overlapping fragments covered the gene from 1307 bp upstream of the translation start site to 625 bp downstream of the stop codon. The lesion identified in *pfl20* changed G2809 (where 1 is the first nucleotide of the initiator codon) of *LON2* to an A, which created an amino acid change (Gly445Arg) and destroyed an *Mnl*I restriction site.

The *PEX6* gene (*At1g0300*) was amplified from *pfl47* genomic DNA using five oligonucleotide pairs (Table 2). The resulting overlapping fragments covered the gene from 151 bp upstream of the translation start site to 346 bp downstream of the stop codon. The lesion identified in *pfl47* changed C1156 (where 1 is the first nucleotide of the initiator codon) of *PEX6* to a T, which created an amino acid change (Leu328Phe).

Identified mutations were followed in the progeny of crosses using PCR amplification with the primers listed in Table 3 followed by digestion of the resultant amplicons with the restriction enzymes indicated in Table 3. The *pex6-1* mutation was followed as previously described (Zolman and Bartel 2004).

Results

Screening for mutants with stabilized GFP–ICL

ICL is a peroxisomal matrix protein that is degraded a few days after *Arabidopsis* seedling germination (Zolman *et al.* 2005; Lingard *et al.* 2009). GFP–ICL driven from the endogenous *ICL* promoter is degraded with similar kinetics as unmodified ICL; GFP–ICL fluorescence, like ICL protein, is no longer apparent 5–6 days after plating (Lingard *et al.* 2009). To isolate mutants with defects in peroxisome-associated protein degradation, we screened for mutants that exhibited prolonged GFP–ICL fluorescence. We mutagenized lines carrying the *ICLp:GFP–ICL* construct with EMS and screened ~44,500 of the resulting M_2 seedlings for GFP–ICL fluorescence that remained visible 7–9 days after plating. We selected 175 putative mutants exhibiting prolonged fluorescence. Of these, 105 died or were infertile, 49 did not display prolonged fluorescence in the M_3 generation, and 21 appeared to prolong GFP–ICL fluorescence in the M_3 generation. We used confocal microscopy to examine GFP–ICL localization in several of these *pfl* mutants. As summarized in Table 4, we found three with extensive cytosolic GFP–ICL fluorescence (Figure 1, F and I), three with punctate GFP–ICL fluorescence similar to the unmutagenized parent (Figure 1, C, E, and G), and three with partially punctate and partially cytosolic GFP–ICL fluorescence (Figure 1, B, D, and H). In addition to these matrix protein localization defects, we observed some aberrations in peroxisome appearance in the mutants. For example, peroxisomes appeared clustered in *pfl7* and *pfl106* (Figure 1, B and H), larger in *pfl20* (Figure 1C), and smaller in *pfl29* (Figure 1D) compared to wild type (Figure 1A).

Peroxisome function in persistent GFP–ICL fluorescence (pfl) mutants

Because defects in peroxisomal matrix protein import often are accompanied by defects in peroxisomal metabolism, we tested peroxisome function in the *pfl* mutants using sucrose dependence and IBA resistance assays, which indirectly assess the efficiency of peroxisomal β-oxidation. Peroxisomal fatty acid β-oxidation provides energy for early seedling development prior to the onset of photosynthesis. Certain peroxisome-defective mutants, such as *pxa1-1* (Zolman *et al.* 2001), arrest or develop slowly following germination because fatty acids are inefficiently metabolized. These defects can be partially bypassed by providing a fixed carbon source, such as

Table 4 Classification of *persistent fluorescence* mutants

Class	Isolate	GFP–ICL fluorescence[a]	ICL stabilization	Sucrose dependence		IBA resistance			PTS2 processing defect[b]
				Light	Dark	Light	Dark	Lateral roots	
—	Wt	P	No	No	No	No	No	No	No
3	*pex4-1 pex22-1* (control)	P	Yes	Yes	Yes	Yes	Yes	Yes	Slight
2	*pfl7/ped1-7*	C and P	Yes	Yes	Yes	Yes	Yes	Yes	Slight
3	*pfl20/lon2-6*	P	No	Slight	Slight	Slight	Slight	Yes	Yes
2	*pfl29*	C and P	Yes	slight	No	Slight	Yes	NT	No
3	*pfl47/pex6-2*	P	Yes	slight	No	Slight	Slight	Yes	No
1	*pfl49/pex14-6*	C	Yes	sight	No	Yes	Yes	Yes	Yes
3	*pfl99*	P	Yes	Yes	Slight	No	No	NT	No
2	*pfl106*	C and P	Yes	Slight	No	No	No	NT	No
1	*pfl164/pfl175/pex14-5*	C	Yes	Yes	Yes	Yes	Yes	Yes	Yes

NT, not tested.
[a] In 4-day-old seedlings; C, cytosolic; P, punctate.
[b] In 8-day-old seedlings.

sucrose, in the growth medium (Hayashi *et al.* 1998; Zolman *et al.* 2000). Four mutants *(pfl7*, *pfl99*, *pfl164*, and *pfl175)* displayed clear sucrose-dependent root elongation in the light (Figure 2A) and/or hypocotyl elongation in the dark (Figure 2B), suggesting inefficient β-oxidation of stored fatty acids, which could result from defects in peroxisome biogenesis or β-oxidation enzymes.

We also compared peroxisome function in the *pfl* mutants using IBA resistance assays. Because the protoauxin IBA is imported into peroxisomes and converted into the active auxin, IAA (reviewed in Strader and Bartel 2011), IBA application reduces primary root elongation (Zolman *et al.* 2000), inhibits hypocotyl elongation in dark-grown seedlings (Strader *et al.* 2008), and promotes proliferation of lateral roots in light-grown seedlings (Zolman *et al.* 2000, 2001, 2007, 2008). When IBA-to-IAA conversion is impaired, the auxin effects of IBA are diminished (Strader *et al.* 2010). Similarly, peroxisomal β-oxidation of the IBA analog 2,4-dichlorophenoxybutyric acid (2,4-DB) to the synthetic auxin 2,4-dichlorophenoxyacetic acid (2,4-D) generates auxin phenotypes (Hayashi *et al.* 1998). Typical peroxin mutants, such as *pex6-1* (Zolman and Bartel 2004), display resistance to the inhibitory effects of IBA (and 2,4-DB) on root elongation in the light and hypocotyl elongation in the dark (Zolman and Bartel 2004; Strader *et al.* 2011). We found that seven *pfl* mutants (*pfl7*, *pfl20*, *pfl29*, *pfl47*, *pfl49*, *pfl164*, and *pfl175*) were IBA (and 2,4-DB) resistant in root (Figure 2A) and/or hypocotyl elongation (Figure 2B), suggesting inefficient β-oxidation of IBA to IAA (and 2,4-DB to 2,4-D) in these mutants.

Mutations in the gene encoding the PEX14 receptor-docking peroxin stabilize GFP–ICL

The three *persistent GFP–ICL fluorescence* mutants with predominantly cytosolic GFP–ICL (*pfl49*, *pfl164*, and *pfl175*; Figure 1 and Table 4) also displayed IBA and 2,4-DB resistance (Figure 2, A and B), consistent with inefficient matrix protein import. Because peroxins facilitate peroxisomal matrix protein import, we examined levels of several peroxins in the *pfl* mutants using immunoblot analysis. We found normal levels of PEX5, PEX6, and PEX7, but reduced levels of full-length PEX14 protein (Figure 2C) in all three mutants with predominantly cytosolic GFP–ICL (Figure 1, F and I). Upon sequencing the *PEX14* gene (*At5g62810*) in these mutants, we identified two novel point mutations, which we renamed *pex14-5* (*pfl164* and *pfl175*) and *pex14-6* (*pfl49*). *pex14-5* changes a Trp to a stop codon in the fourth exon (Figure 3A). Overexposure of an anti-PEX14 immunoblot

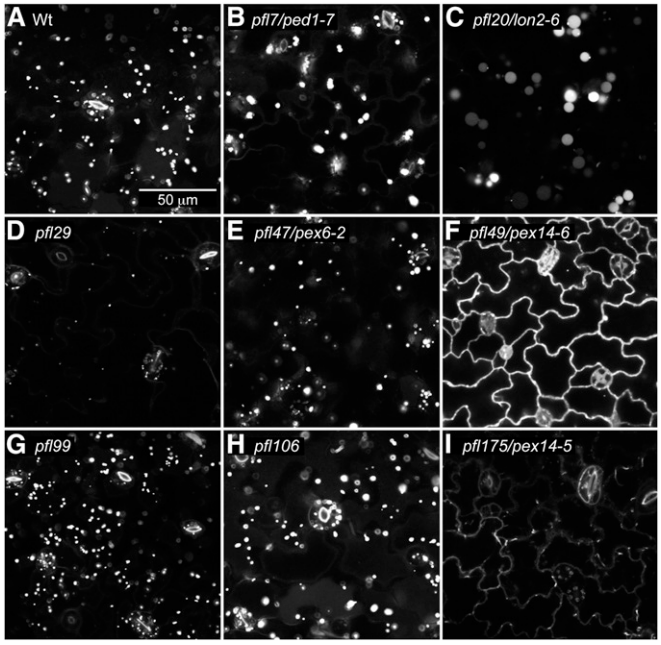

Figure 1 Localization of GFP–ICL using confocal microscopy separates *pfl* mutants into three categories: (1) cytosolic, (2) both cytosolic and punctate, and (3) punctate patterns. Cotyledon epidermal cells of 4-day-old light-grown Wt (Col-0 transformed with *ICLp:GFP-ICL*) (A) or *pfl* mutant (B–I) seedlings were imaged for GFP using confocal microscopy. *pfl20/lon2-6* (C), *pfl47/pex6-2* (E), and *pfl99* (G) display punctate GFP–ICL fluorescence characteristic of peroxisomal localization. Cytosolic GFP–ICL is visible at the cell margins in *pfl49/pex14-6* (F) and *pfl175/pex14-5* (I). *pfl7/ped1-7* (B), *pfl29* (D), and *pfl106* (H) display both punctate and cytosolic localization. This experiment was repeated twice with similar results. Scale bar, 50 μm.

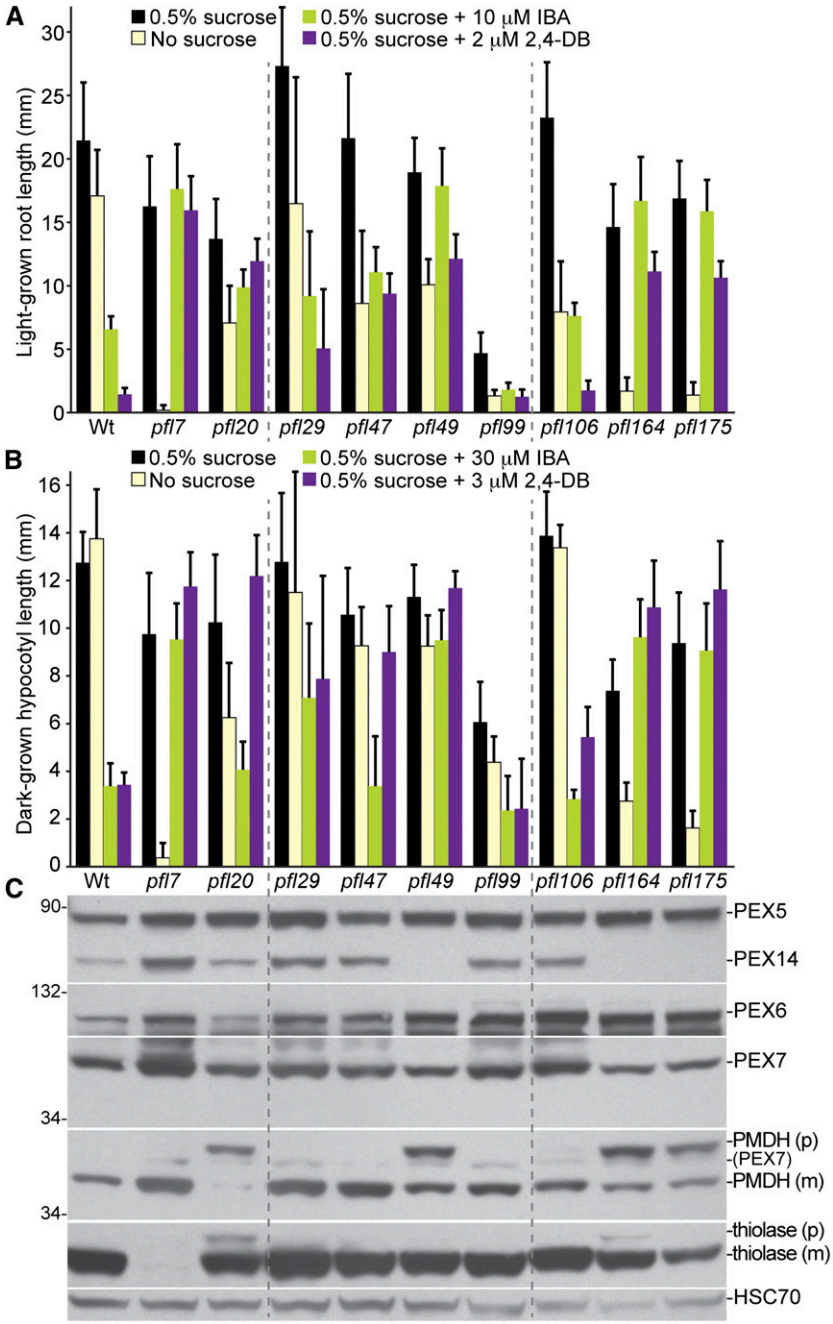

Figure 2 Most *pfl* mutants display physiological and/or molecular defects suggestive of peroxisomal defects. (A) Root lengths of 8-day-old *pfl* or Wt (Col-0) seedlings grown in yellow light in the presence or absence of sucrose or on sucrose-supplemented medium containing inhibitory concentrations of IBA or 2,4-DB are shown. Error bars show standard deviations of the means ($n \geq 12$). (B) Hypocotyl lengths of 6-day-old *pfl* or Wt (Col-0) seedlings grown in the dark in the presence or absence of sucrose or on sucrose-supplemented medium containing inhibitory concentrations of IBA or 2,4-DB are shown. Error bars show standard deviations of the means ($n \geq 12$). (C) Protein extracts from the 8-day-old seedlings grown in the light on 0.5% sucrose (in A) were processed for immunoblotting. The membrane was serially probed with antibodies to the indicated proteins. The positions of molecular mass markers (in kilodaltons) are indicated at the left. PMDH and thiolase (PED1) are synthesized as precursors (p) containing the PTS2 signal that is processed into the mature (m) protein in peroxisome. Residual PEX7 (PEX7) from a previous probing remains visible in the PMDH panel. HSC70 is a loading control. Experiments in A through C were repeated twice with similar results.

did not reveal PEX14 protein in *pex14-5* seedlings (Figure 3D), suggesting that *pex14-5* is a null allele. *pex14-6* harbors a mutation in the last nucleotide of exon 1, which would change Glu25 to Lys and disrupt a slice site (Figure 3A), and accumulates a small amount of nearly full-length PEX14 protein (Figure 3D). We isolated RNA from the *pex14-6* mutant and determined that the major *pex14-6* splice product uses a cryptic 5′-donor site in the 5′-UTR, thereby skipping the first exon of *PEX14*.

We compared these two new *pex14* alleles to several previously characterized *pex14* alleles (Monroe-Augustus *et al.* 2011) and found that the new alleles conferred similar IBA and 2,4-DB resistance in both dark- and light-grown seedlings (Figure 3, B and C) along with transient defects in removal of the PTS2-containing presequence from the matrix protein thiolase (Figure 3E). Unlike other *pex14* alleles, the *pex14-6* allele was not dependent on sucrose in the dark (Figure 3B), suggesting that the low level of *pex14-6* protein detected in this mutant (Figure 3D) retained partial PEX14 function.

To assess whether disruption of PEX14 stabilizes endogenous peroxisomal matrix proteins, we compared ICL stability in wild type, *pex14-5*, *pex14-6*, and *pex14-2*, a previously described *pex14* null allele (Monroe-Augustus *et al.* 2011). We found that ICL protein was stabilized in all three *pex14* alleles compared to wild type (Figure 3E). Our

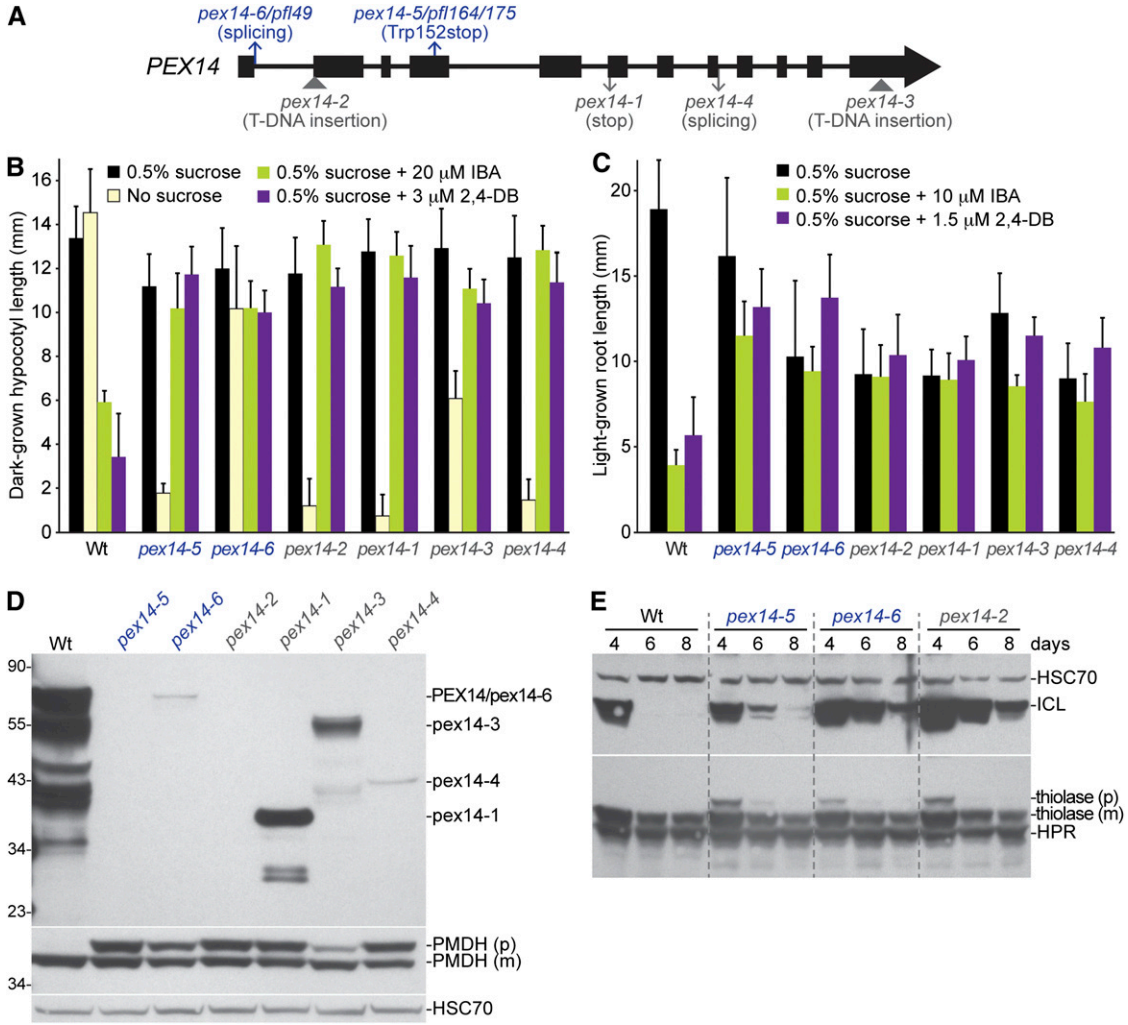

Figure 3 *pex14* mutants display physiological and molecular peroxisomal defects and stabilize ICL. (A) Positions of newly identified *pfl* alleles are shown above and characterized alleles are shown below a *PEX14* gene model in which exons are shown as boxes and introns as lines. (B) Hypocotyl lengths of 7-day-old *pfl* or Wt (Col-0 transformed with *ICLp:GFP-ICL*) seedlings grown in the dark in the presence or absence of sucrose or on sucrose-supplemented medium containing inhibitory concentrations of IBA or 2,4-DB are shown. Error bars show standard deviations of the means ($n \geq 10$). (C) Root lengths of 8-day-old seedlings *pfl* or Wt (Col-0 transformed with *ICLp:GFP-ICL*) grown under yellow-filtered light on sucrose-supplemented medium containing inhibitory concentrations of IBA or 2,4-DB are shown. Error bars show standard deviations of the means ($n \geq 10$). (D) Protein extracts from the 8-day-old seedlings grown in the light on 0.5% sucrose in C were processed for immunoblotting. The membrane was serially probed with antibodies to the indicated proteins. The positions of molecular mass markers (in kilodaltons) are indicated at the left. An overexposed anti-PEX14 immunoblot revealed PEX14 protein in all *pex14* alleles except *pex14-5* and *pex14-2*. PMDH is synthesized as a precursor (p) with a cleavable PTS2 signal that is processed into mature (m) PMDH in the peroxisome; this cleavage is impaired in *pex14* mutants. HSC70 is a loading control. (E) ICL is stabilized in *pex14* mutants. Protein extracts from 4-, 6-, and 8-day-old light-grown Wt (Col-0) and *pex14* seedlings were processed for immunoblotting. The membrane was serially probed with antibodies to the indicated proteins. Thiolase is synthesized as a precursor (p) with a cleavable PTS2 signal that is processed into mature (m) thiolase in the peroxisome. HSC70 is a loading control. Experiments in B through E were repeated twice with similar results.

recovery of *pex14* alleles as *persistent GFP–ICL fluorescence* mutants suggests that impaired peroxisome matrix protein import prevents access of GFP–ICL and ICL to the peroxisome-associated proteolysis machinery or the factors or conditions needed to target substrates to this machinery.

A mutation in a gene encoding the LON2 peroxisomal protease

The *pfl20* mutant displayed punctate GFP–ICL fluorescence in 4-day-old seedlings (Figure 1C). We used the associated phenotype of IBA-resistant primary root elongation (Figure 2A) to map the *pfl20* lesion to an interval on the bottom of chromosome 5 (Figure 4) that included the gene encoding the LON2 (At5g47040) peroxisomal ATP-dependent protease (Lingard and Bartel 2009). We sequenced *LON2* from *pfl20* genomic DNA and found a point mutation in exon 10 (Figure 5A) that changed Gly445 to an Arg residue. The mutated Gly residue is in the AAA–ATPase domain (Figure 5A) between the Walker A and B domains and is invariant in LON isoforms from plants, fungi, bacteria, and mammals. Like other *lon2* alleles (Lingard and Bartel 2009), *pfl20* displayed moderate resistance to the inhibition of root and

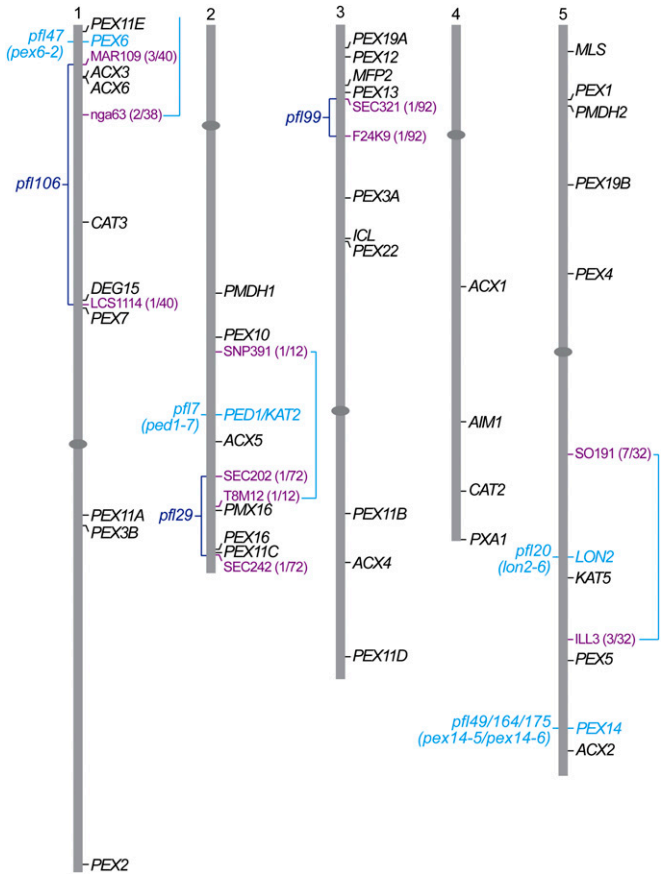

Figure 4 Map positions of *pfl* mutants were determined using recombination mapping. Map positions of genes encoding peroxins and selected additional peroxisomal proteins (in black) and bordering mapping markers used (in lavender) are shown to the right of the five *Arabidopsis thaliana* chromosome. Identified *pfl* mutants (in turquoise) and unidentified *pfl* mutants (in dark blue) are shown to the left of the chromosomes with mapping intervals bracketed and the number of recombinants/number of chromosomes scored shown in parentheses (in lavender).

hypocotyl elongation by IBA (Figure 5, B and C), severe resistance to the promotive effects of IBA on lateral rooting (Figure 5D), and PMDH PTS2 processing defects (Figure 5E). We renamed this mutant *lon2-6*.

Because LON2 is a peroxisomal protease (Ostersetzer *et al.* 2007), it was a candidate for participation in peroxisome-associated protein degradation. However, previously characterized *lon2* T-DNA insertion alleles do not dramatically stabilize ICL or MLS (Lingard and Bartel 2009). To examine whether peroxisomal matrix proteins were stabilized in the *lon2-6* mutant, we compared ICL stability in wild type, *lon2-6*, and *lon2-2*, a previously characterized (Lingard and Bartel 2009) *lon2* allele disrupted by a T-DNA insertion near the 3′ end of the gene (Figure 5A). Indeed, we found that ICL was not stabilized in either *lon2* mutant compared to wild type (Figure 5E). Some *lon2* alleles display uneven germination (Lingard and Bartel 2009), suggesting that a germination delay of the M_2 seedling may explain our original isolation of the *pfl20/lon2-6* mutant in the *persistent GFP–ICL fluorescence* screen.

Mutations in the PED1 gene encoding a peroxisomal thiolase stabilize GFP–ICL

pfl7 displayed a combination of peroxisomal and cytosolic GFP–ICL fluorescence (Figure 1B) and the classical peroxisome-defective phenotypes of IBA- and 2,4-DB-resistant root and hypocotyl elongation and sucrose-dependent seedling development (Figure 2, A and B). We used the sucrose-dependence phenotype to map the *pfl7* lesion to a region of chromosome 2 that included *PED1* (*At2g33150*; Figure 4), which encodes a peroxisomal 3-ketoacyl-CoA thiolase, also known as KAT2, that is implicated in fatty acid, IBA, and 2,4-DB β-oxidation (Hayashi *et al.* 1998; Germain *et al.* 2001). In addition, we did not detect thiolase protein on immunoblots of *pfl7* seedling extracts (Figure 2C). We sequenced *PED1* from *pfl7* DNA and found a point mutation in the first nucleotide of intron 10 that is predicted to disrupt *PED1* splicing (Figure 5A). The nature of the lesion was consistent with the lack of full-length thiolase (PED1) protein detected in immunoblots of *pfl7* seedling extracts (Figures 2C and 5E), and we renamed *pfl7* as *ped1-7*.

We found that *ped1-7* displayed β-oxidation defects similar in severity to *ped1-96* (Figure 5, B-D), a previously isolated *ped1* null allele (Lingard and Bartel 2009). However, matrix protein import defects have not been reported for *ped1-96* (Lingard and Bartel 2009), the original *ped1* allele (Hayashi *et al.* 1998), or the *kat2-1* T-DNA insertion allele of *PED1* (Germain *et al.* 2001). Because *ped1-7* partially mislocalized GFP–ICL to the cytosol (Figure 1B), we examined PTS2 processing in *ped1* mutants. We found that both *ped1-7* and *ped1-96* displayed a slight defect in PTS2 processing of PMDH (Figure 5E), consistent with the slight defect in matrix protein import revealed by the partial mislocalization of GFP–ICL to the cytosol in *ped1-7* (Figure 1B).

To examine whether disruption of the PED1 thiolase stabilizes endogenous peroxisomal matrix proteins, we compared ICL stability in wild type, *ped1-7*, and *ped1-96*. We found that ICL was similarly stabilized in both *ped1* alleles (Figure 5E). To examine whether this stabilization might reflect a developmental delay caused by the reduced fatty acid β-oxidation that would result from reduced thiolase activity, we monitored the timing of appearance of the photorespiration enzyme hydroxypyruvate reductase (HPR) in the *ped1* mutants. In wild-type seedlings, HPR appears during the transition to photosynthetic growth as ICL is degraded (Lingard *et al.* 2009). We found that HPR appeared in *ped1* mutants with similar timing as in wild type (Figure 5E), suggesting that *ped1* developmental delays did not account for the observed ICL stabilization (Figure 5E).

The PEX6 AAA–ATPase is required for efficient peroxisome-associated degradation

The *pfl47* mutant displayed normal peroxisomal localization of GFP–ICL (Figure 1E) and normal levels of assayed peroxins (Figure 2C). We used the persistent GFP–ICL fluorescence phenotype to map *pfl47* to a region at the top of

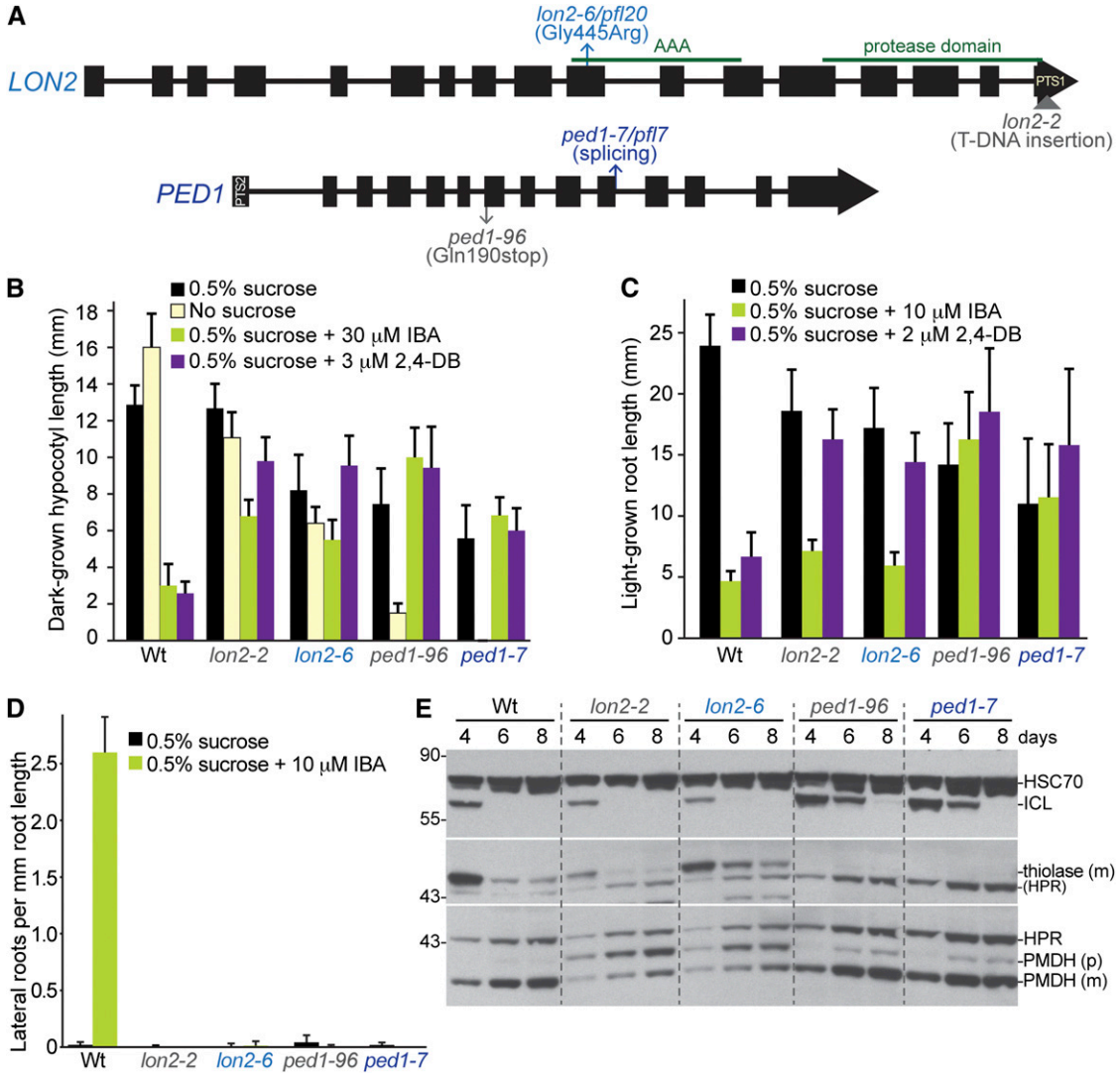

Figure 5 Both *lon2* and *ped1* mutants display physiological and molecular peroxisomal defects, but only *ped1* mutants stabilize ICL. (A) Positions of newly identified *pfl* alleles are shown above and characterized alleles are shown below gene models of *LON2* and *PED1*. Green lines above the *LON2* gene model delineate regions encoding the central AAA domain and the C-terminal protease domain. *LON2* and *PED1* encode proteins that are targeted to peroxisomes via a C-terminal PTS1 signal or an N-terminal PTS2 signal, respectively. (B) Hypocotyl lengths of 6-day-old *pfl* or Wt (Col-0) seedlings grown in the dark in the presence or absence of sucrose or on sucrose-supplemented medium containing inhibitory concentrations of IBA or 2,4-DB are shown. Error bars show standard deviations of the means ($n \geq 12$). (C) Root lengths of 8-day-old *pfl* or Wt (Col-0) seedlings grown under yellow-filtered light on sucrose-supplemented medium containing inhibitory concentrations of IBA or 2,4-DB are shown. Error bars show standard deviations of the means ($n \geq 15$). (D) Lateral roots per millimeter of root length of 8-day-old *pfl* or Wt (Col-0) seedlings 4 days after transfer to sucrose-containing medium with or without 10 μM IBA are shown. Error bars show standard deviations of the means ($n \geq 8$). (E) ICL is stabilized in *ped1* mutants but is degraded similarly to wild type in *lon2* mutants. Protein extracts from 4-, 6-, and 8-day-old light-grown Wt (Col-0) and mutant seedlings were processed for immunoblotting. The membrane was serially probed with antibodies to the indicated proteins. The positions of molecular mass markers (in kilodaltons) are indicated at the left. PMDH and thiolase are synthesized as precursors (p) with a cleavable PTS2 signal that are processed into mature (m) versions in the peroxisome. Residual HPR (HPR) from a previous probing remains visible in the thiolase panel. HSC70 is a loading control. Experiments in B, C, and E were repeated twice with similar results.

chromosome 1 that included the *PEX6* gene (*At1g03000*; Figure 4). Upon sequencing *PEX6* from *pfl47* DNA, we found a point mutation in exon 3 that changed Leu328 to a Phe residue (Figure 6A). We renamed *pfl47* as *pex6-2*. We compared the phenotypes of *pex6-2* to those of *pex6-1*, a different missense allele isolated in a screen for mutants displaying IBA-resistant root elongation that also is sucrose dependent and displays a marked PTS2 processing defect (Zolman and Bartel 2004). Unlike *pex6-1*, *pex6-2* developed normally in the absence of sucrose in the dark (Figure 6B), was only moderately resistant to the inhibitory effects of IBA on hypocotyl (Figure 6B) or root (Figure 6C) elongation, processed the PTS2 proteins thiolase and PMDH nearly normally (Figures 2C and 6E), and displayed a wild-type root length on sucrose-supplemented medium (Figure 6C). Both *pex6* alleles displayed clear resistance to the inhibitory

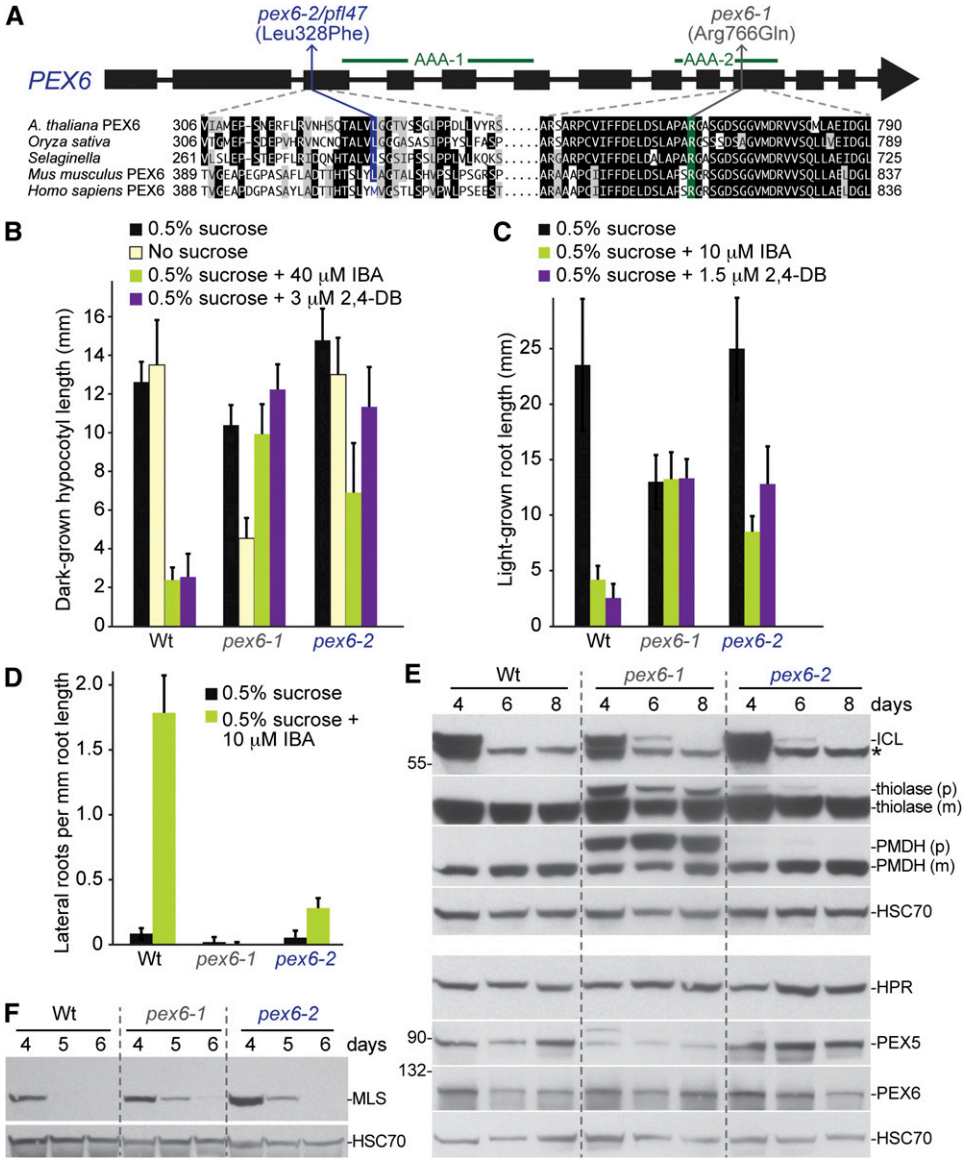

Figure 6 *pex6-2* and *pex6-1* display partially overlapping physiological and molecular peroxisomal defects and stabilize ICL and MLS. (A) The positions of the newly identified *pfl47/pex6-2* allele and the characterized *pex6-1* allele are shown above a gene model of *PEX6*. Green lines above the gene model delineate regions encoding the two PEX6 AAA domains. *Arabidopsis* PEX6 regions containing the *pex6-2* and *pex6-1* lesions are shown below the gene model aligned with orthologs from *Oryza sativa* (NP_001053886), *Selaginella moellendorffii* (XP_002979987), *Mus musculus* (NP_663463), and *Homo sapiens* (NP_000278). (B) Hypocotyl lengths of 6-day-old *pfl* or Wt (Col-0 transformed with *ICLp:GFP-ICL*) seedlings grown in the dark in the presence or absence of sucrose or on sucrose-supplemented medium containing inhibitory concentrations of IBA or 2,4-DB are shown. Error bars show standard deviations of the means ($n \geq 10$). (C) Root lengths of 8-day-old *pfl* or Wt (Col-0 transformed with *ICLp:GFP-ICL*) seedlings grown under yellow-filtered light on sucrose-supplemented medium containing inhibitory concentrations of IBA or 2,4-DB are shown. Error bars show standard deviations of the means ($n \geq 8$). (D) Lateral roots per millimeter root length of 8-day-old *pfl* or Wt (Col-0) seedlings 4 days after transfer to sucrose-containing medium with or without 10 μM IBA are shown. Error bars show standard deviations of the means ($n \geq 8$). (E) Both *pex6* alleles stabilize ICL, whereas only *pex6-1* displays reduced PEX5 levels or severe PTS2 processing defects. Protein extracts from 4-, 6-, and 8-day-old light-grown Wt (Col-0 transformed with *ICLp:GFP-ICL*) or mutant seedlings were processed for immunoblotting. Membranes from duplicate gels were serially probed with antibodies to the indicated proteins to obtain the top four panels and the bottom four panels. The positions of molecular mass markers (in kilodaltons) are indicated at the left. PMDH and thiolase are synthesized as precursors (p) with a cleavable PTS2 signal that is processed into mature (m) versions in the peroxisome. An asterisk marks a cross-reacting band detected by the ICL antibody that is not present in an *icl* null mutant (Lingard *et al.* 2009). HSC70 is a loading control. (F) Both *pex6* alleles stabilize MLS. Protein extracts from 4-, 5-, and 6-day-old Wt (Col-0 transformed with *ICLp:GFP-ICL*) or mutant light-grown seedlings were processed for immunoblotting with antibodies to MLS and HSC70, a loading control. Experiments in B through F were repeated at least twice with similar results.

effects of 2,4-DB on hypocotyl elongation in the dark (Figure 6B) and to the promotive effects of IBA on lateral root formation in the light (Figure 6D). Moreover, both alleles similarly stabilized ICL and MLS (Figure 6, E and F). Because the *pex6-2* phenotypes were not identical to those of *pex6-1*, we introduced a wild-type genomic copy of *PEX6* (Zolman and Bartel 2004) into *pex6-2* using *Agrobacterium*-mediated transformation to ensure that the identified *pex6-2* lesion was responsible for the phenotypes observed. We found that this *PEX6p:PEX6* construct rescued the 2,4-DB (Figure 7A) and IBA resistance (Figure 7B) of *pex6-2* and *pex6-1*, confirming that the identified *pex6-2* lesion caused the peroxisome-defective phenotypes observed.

To further define the extent of the differences between the *pex6-1* and *pex6-2* alleles, we compared the effects of overexpressing human PEX6 or *Arabidopsis* PEX5 in these mutants. The *pex6-1* mutation alters an Arg residue in the second AAA domain (Figure 6A) that is conserved in human PEX6 (Zolman and Bartel 2004), whereas the Leu residue mutated in *pex6-2* is a Met in the human protein and is in a less conserved region (Figure 6A). Expression of a human *PEX6* cDNA from the cauliflower mosaic virus *35S* promoter (*35S:HsPEX6*) rescues the IBA resistance and sucrose dependence of *pex6-1* (Zolman and Bartel 2004). Similarly, we found that expressing this human *PEX6* cDNA restored *pex6-1* sensitivity to lateral root promotion by IBA (Figure

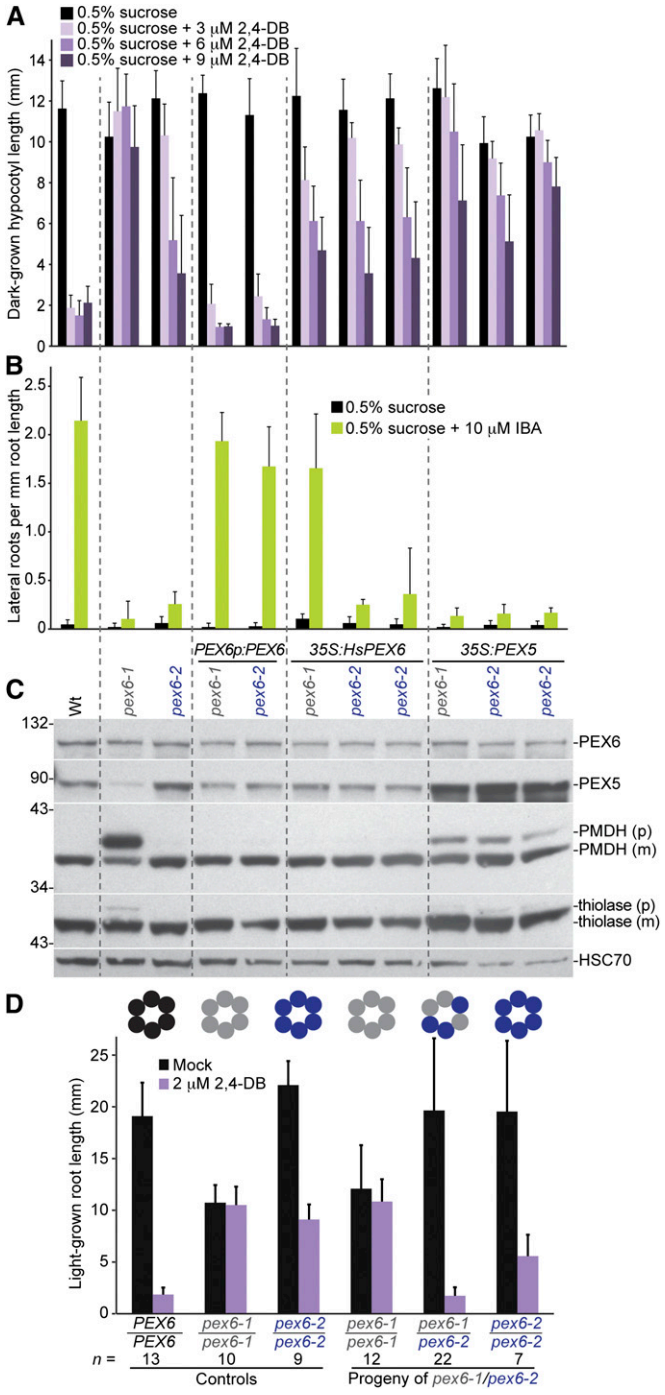

Figure 7 *pex6* complementation analysis. (A) The 2,4-DB resistance of *pex6-1* is fully rescued by the *pBINPEX6* genomic *Arabidopsis PEX6* construct (*PEX6p:PEX6*) and partially rescued by expression of a human *PEX6* cDNA (*35S:HsPEX6*) or *Arabidopsis PEX5* overexpression (*35S:PEX5*), whereas *pex6-2* 2,4-DB resistance is rescued by the genomic *PEX6* construct, unaffected by expression of human *PEX6* (two transformants shown), and enhanced by *Arabidopsis PEX5* overexpression (two transformants shown). Hypocotyl lengths of 6-day-old Wt (Col-0) or mutant seedlings grown in the dark on sucrose-supplemented medium containing increasing concentrations of 2,4-DB are shown. Error bars show standard deviations of the means ($n \geq 15$). (B) The IBA resistance of both *pex6-1* and *pex6-2* lateral root production is fully rescued by a genomic *Arabidopsis PEX6* construct but not by *Arabidopsis PEX5* overexpression. Human *PEX6* expression restores IBA-responsive lateral rooting to *pex6-1* but not to *pex6-2* (two transformants shown). Lateral roots per millimeter root length of 8-day-old Wt (Col-0) or mutant seedlings 4 days after transfer to sucrose-containing medium with or without 10 μM IBA are shown. Error bars show standard deviations of the means ($n \geq 8$). (C) The PTS2 processing defect and reduced PEX5 levels of *pex6-1* are rescued by a genomic *Arabidopsis PEX6* construct and by expression of human *PEX6* and are partially rescued by *Arabidopsis PEX5* overexpression; *pex6-2* acquires PTS2 processing defects when *Arabidopsis PEX5* is overexpressed. Protein extracts from the 8-day-old light-grown control seedlings from B were processed for immunoblotting. The membrane was serially probed with antibodies to the indicated proteins. The positions of molecular mass markers (in kilodaltons) are indicated at the left. PMDH and thiolase are synthesized as precursors (p) with a cleavable PTS2 signal that are processed into mature (m) proteins in the peroxisome. HSC70 is a loading control. (D) *pex6-1* and *pex6-2* exhibit intragenic complementation of 2,4-DB resistant root elongation. Control and F_2 progeny were plated on media without and with 2,4-DB and root lengths of 8-day-old seedlings were measured. The genotype of each seedling was then determined. The number of seedlings (n) of each genotype is indicated. This intragenic complementation suggests that the *pex6-1* and *pex6-2* missense lesions affect different PEX6 functions and that mixed oligomers with both pex6-1 (gray circles) and pex6-2 (purple circles) can carry out PEX6 (black circles) functions. Experiments in A, C, and D were repeated at least twice with similar results.

7B), rescued *pex6-1* PTS2 processing defects (Figure 7C), and partially restored sensitivity of *pex6-1* hypocotyls to 2,4-DB in the dark (Figure 7A). In marked contrast, *35S:HsPEX6* did not rescue the strong resistance of *pex6-2* lateral roots to IBA (Figure 7B) or the partial resistance of *pex6-2* hypocotyls to 2,4-DB (Figure 7A). Our observation that *35S:HsPEX6* failed to rescue the *pex6-2* phenotypes assayed suggests that the function(s) disrupted by the *pex6-2* mutation is not conserved in the human protein (Figure 6A), unlike the *pex6-1* mutation (Zolman and Bartel 2004).

pex6-1 exhibits reduced PEX5 levels (Zolman and Bartel 2004), probably because PEX5 is polyubiquitinated and degraded when it is not efficiently removed from the peroxisome by PEX6. *PEX5* overexpression from the *35S* promoter (*35S:PEX5*) partially suppresses the sucrose dependence and growth defects of *pex6-1* without restoring IBA sensitivity (Zolman and Bartel 2004). In addition, we found that *PEX5* overexpression partially restored PTS2 processing in *pex6-1* (Figure 7C). Unlike *pex6-1*, we found normal PEX5 levels in *pex6-2* (Figures 2C, 6E, and 7C). In contrast to the beneficial effects of *PEX5* overexpression in *pex6-1* (Figure 7, A and C), *PEX5* overexpression enhanced *pex6-2* 2,4-DB resistance (Figure 7A) and induced a PTS2 processing defect in *pex6-2* (Figure 7C). These enhancements of *pex6-2* defects by *PEX5* overexpression suggest that unlike *pex6-1*, *pex6-2* defects are not caused by lack of PEX5 available to escort proteins into the peroxisome.

Because the *pex6-1* and *pex6-2* alleles performed differently in a variety of assays (Figure 6, B–E, and Figure 7, A–C), we assessed the ability of each *pex6* lesion to complement the defects of the other. F_2 plants from a cross of *pex6-1* and *pex6-2* were assayed for 2,4-DB resistance in roots and individual plants were genotyped. Surprisingly,

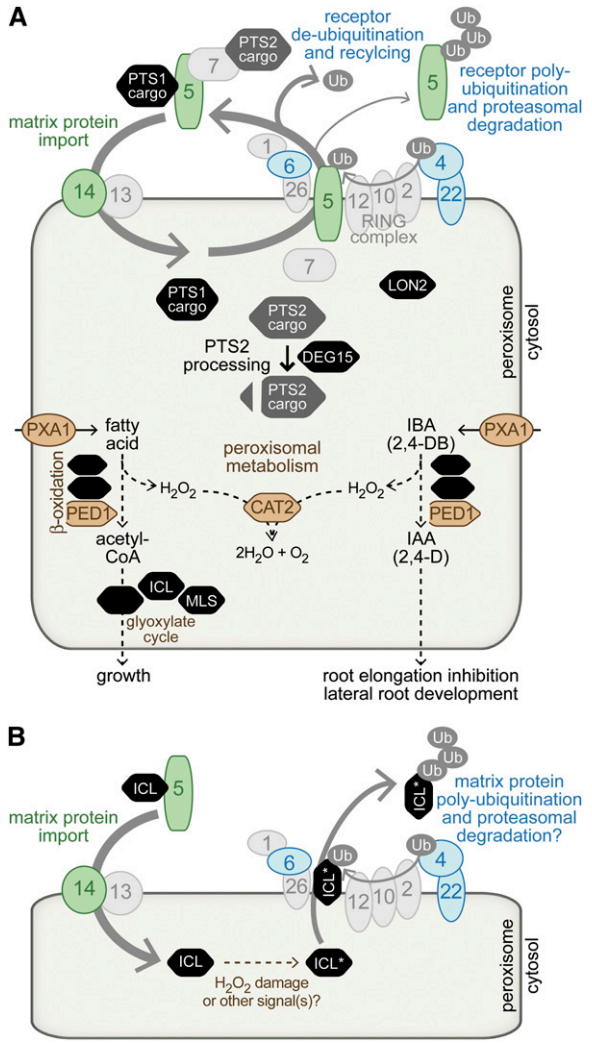

Figure 8 *Arabidopsis* peroxisomal matrix protein degradation is influenced by proteins implicated in matrix protein import, receptor recycling, and peroxisomal metabolism. (A) Likely functions of *Arabidopsis* peroxins (numbered ovals) in peroxisome matrix protein import based on data from *Arabidopsis* and other systems (reviewed in Hu *et al.* 2012). Matrix proteins are targeted to the peroxisome via a C-terminal PTS1 or an N-terminal PTS2, which are recognized in the cytosol by the PEX5 and PEX7 receptors, respectively. Receptors dock with the membrane peroxins PEX13 and PEX14, deliver cargo, and are recycled. PEX5 recycling requires the ubiquitin-conjugating enzyme PEX4 and a RING-finger complex composed of PEX2, PEX10, and PEX12. The PEX6 and PEX1 AAA–ATPases promote retrotranslocation of ubiquitinated PEX5 out of the peroxisome; in the absence of efficient recycling, PEX5 can be multi-ubiquitinated and degraded in the proteasome. Once in the peroxisome, PTS2 proteins are processed by the peroxisomal protease DEG15 (Helm *et al.* 2007; Schumann *et al.* 2008). Both PTS2 and PTS1 proteins contribute to peroxisome metabolism, including fatty acid and IBA β-oxidation, exemplified by PED1 (Hayashi *et al.* 1998; Zolman *et al.* 2000), the glyoxylate cycle, exemplified by ICL (Eastmond *et al.* 2000a) and MLS (Cornah *et al.* 2004), and H_2O_2 decomposition by catalases including CAT2. PXA1 is a membrane protein that likely transports fatty acids and IBA into the peroxisome (Zolman *et al.* 2001). Mutants defective in proteins shown in color alter the degradation rate of glyoxylate cycle enzymes, including proteins involved in matrix protein import (green), receptor recycling components (blue), and proteins involved in peroxisomal metabolism (brown). (B) A model for peroxisomal matrix protein degradation. Efficient ICL degradation requires PEX5 (Lingard *et al.* 2009) and PEX14 (this work), implying that ICL import into the peroxisome precedes ICL degradation. Once in the peroxisome, peroxisome metabolism influences the ICL degradation rate, perhaps by modulating the extent of H_2O_2 damage. For example, ICL degradation is slowed in *ped1* (this work) and *pxa1* (Lingard *et al.* 2009) and is enhanced in a *cat2* mutant (Lingard *et al.* 2009). The stabilization of ICL (and MLS) in the *pex4-1 pex22-1* mutant (Lingard *et al.* 2009) and *pex6* mutants (this work) is consistent with the possibility that ICL may exit the peroxisome for cytosolic degradation in the proteasome.

we found that *pex6-1/pex6-2* seedlings were as sensitive to 2,4-DB as wild-type *PEX6/PEX6* seedlings were (Figure 7D). This intragenic complementation is consistent with our observation that both *pex6* alleles accumulated wild-type levels of pex6 protein (Figures 6E and 7C) and implied that the two missense mutations affect separable functions of PEX6.

Additional pfl mutants

We used recombination mapping to localize *pfl29*, *pfl99*, and *pfl106* to distinct chromosome regions (Figure 4). We mapped the *pfl29* lesion to the bottom of chromosome 2, using persistent GFP–ICL fluorescence phenotype, *pfl99* to the top of chromosome 3 using the associated phenotype of sucrose dependence, and *pfl106* to a region on chromosome 1 using the persistent GFP–ICL fluorescence phenotype (Figure 4). These mapping data indicate that additional loci can mutate to confer GFP–ICL stabilization. Map-based cloning of these additional loci is ongoing.

Discussion

Three classes of pfl mutants based on subcellular GFP–ICL localization

Although much is known about how matrix proteins enter peroxisomes (reviewed in Hu *et al.* 2012), little is known about how these matrix proteins are ultimately degraded. The developmentally controlled degradation of the glyoxylate cycle enzymes ICL and MLS provides model substrates with which to unravel peroxisome-associated degradation. We have begun isolating and characterizing mutants with impaired degradation of a GFP–ICL reporter, anticipating that analysis of the defective genes will elucidate the mechanism of peroxisomal matrix protein degradation. We selected mutants that retained GFP–ICL fluorescence longer than wild type, and subcellular GFP–ICL localization has allowed us to separate the mutants into different classes. The first class contains mutants with predominantly cytosolic GFP–ICL, mutants in the second class display both cytosolic and punctate GFP–ICL, and the third class includes mutants with predominantly punctate GFP–ICL (Table 4).

Import into the peroxisome is needed for efficient ICL degradation

The *pex14-5* and *pex14-6* mutants are members of the first class of *pfl* mutants (Table 4). As illustrated in Figure 8A, PEX14 is a peroxisomal membrane protein (Hayashi *et al.*

2000) that acts with PEX13 as the PEX5–PEX7 docking complex (Schell-Steven *et al.* 2005) and may assist PEX5 in forming a transient matrix protein import pore (Meinecke *et al.* 2010). Whereas *pex14-5* resembles previously described *pex14* null alleles (Hayashi *et al.* 2000; Monroe-Augustus *et al.* 2011), *pex14-6* is unique among described *Arabidopsis pex14* mutants in displaying sucrose independence (Figure 3B), suggesting that residual *pex14-6* protein (Figure 3D) retains some PEX14 function. The viability of the *pex14-5* apparent null allele (Figure 3D) confirms a recent report that PEX14, unlike its docking partner PEX13 (Boisson-Dernier *et al.* 2008), is not required for *Arabidopsis* viability (Monroe-Augustus *et al.* 2011). All of the assayed *pex14* alleles similarly stabilize ICL (Figure 3E). ICL and MLS also are stabilized in the *pex5-10* mutant (Lingard *et al.* 2009), another peroxin mutant that displays severe matrix protein import defects (Khan and Zolman 2010). These demonstrations that ICL and MLS must enter the peroxisome to be efficiently degraded suggest that either the degradation machinery or the machinery needed to target ICL for destruction is peroxisome associated (Figure 8B).

Peroxisomal metabolism can influence ICL degradation

We found that PED1 promotes efficient peroxisomal matrix protein degradation (Figure 5E). PED1 is a peroxisomal thiolase (Figure 8A) needed for β-oxidation of fatty acids to acetyl-CoA (Hayashi *et al.* 1998) and of IBA to IAA (Zolman *et al.* 2000). We were surprised to find that PED1 also was needed for efficient matrix protein import, as judged by both incomplete removal of the PTS2-containing sequence from PMDH (Figure 5E) and partial GFP–ICL mislocalization to the cytosol (Figure 1B) in *ped1* mutants. *ped1* mutants have larger peroxisomes than wild type (Hayashi *et al.* 1998); perhaps this altered geometry physically impairs matrix protein import. Alternatively, there may exist an undiscovered feedback mechanism linking matrix protein import with peroxisomal metabolism. In either case, ICL stabilization in *ped1* mutants might result from inefficient import of ICL into the peroxisome matrix, as in the *pex14* and *pex5-10* mutants discussed above. Arguing against this possibility is our observation that *lon2* mutants, which display more severe PTS2 processing defects than *ped1* mutants display, fail to stabilize ICL (Figure 5E). An alternative possibility is that reduced β-oxidation in *ped1* lowers peroxisomal H_2O_2, reducing oxidative damage and slowing degradation. Indeed, ICL and MLS are similarly stabilized in a *pxa1* mutant (Lingard *et al.* 2009) that shows complete sucrose dependence, strong IBA resistance (Zolman *et al.* 2001), and reduced H_2O_2 levels (Eastmond 2007) due to a reduced ability to move β-oxidation substrates into the peroxisome (Figure 8A). Conversely, ICL and MLS degradation is hastened in the *cat2* mutant (Lingard *et al.* 2009), which is missing one of the peroxisomal catalases that decompose H_2O_2. A third nonexclusive possibility is that ICL and MLS degradation may be linked to the depletion of seedling fatty acid stores, which also would explain our observations that ICL degradation is delayed in several mutants with impaired fatty acid β-oxidation. For example, ICL and MLS degradation might be inhibited by fatty acids or β-oxidation intermediates or might be promoted by sucrose or other downstream metabolites of β-oxidation.

The PEX6 ATPase is needed for efficient matrix protein degradation

As illustrated in Figure 8A, PEX4 is a ubiquitin-conjugating enzyme that in yeast and plants is tethered to the peroxisome by PEX22 (Koller *et al.* 1999; Zolman *et al.* 2005) and in yeast provides ubiquitin to RING finger peroxins that ubiquitinate the matrix protein receptor PEX5 (Thoms and Erdmann 2006; Platta *et al.* 2007, 2009). PEX6 and PEX1 are AAA–ATPases that in yeast and mammals assist in the retrotranslocation of ubiquitinated PEX5 from the peroxisome (Figure 8A), thus recycling PEX5 for further import rounds (reviewed in Fujiki *et al.* 2012; Grimm *et al.* 2012); PEX5 is poly-ubiquitinated and degraded in the proteasome when PEX6 is not functional (Platta *et al.* 2007). *Arabidopsis* PEX6 likely functions similarly to its yeast and mammalian orthologs, as the *pex6-1* allele has decreased PEX5 levels and is partially rescued by PEX5 overexpression (Figure 7C and Zolman and Bartel 2004).

By screening for GFP–ICL stabilization, we identified a novel *pex6* allele, *pex6-2*, that shares only a subset of *pex6-1* defects, including IBA and 2,4-DB resistance (Figure 6, B-D). Unlike *pex6-1*, *pex6-2* did not require sucrose for normal development in the dark (Figure 6B), processed PTS2 proteins nearly as efficiently as wild type (Figure 6E), and had normal PEX5 levels (Figures 2C, 6E, and 7C). Moreover, *pex6-2* physiological and molecular defects were exacerbated rather than rescued by PEX5 overexpression (Figure 7, A and C). Interestingly, the *pex6-1* and *pex6-2* lesions were able to complement one another (Figure 7D). PEX6 is thought to function as a hexamer (reviewed in Fujiki *et al.* 2012; Grimm *et al.* 2012), and this intragenic complementation suggests that the *pex6-1* and *pex6-2* missense lesions affect different PEX6 functions, allowing mixed pex6-1 pex6-2 oligomers to carry out all PEX6 functions. Like *pex4-1 pex22-1* and *pex6-1* (Lingard *et al.* 2009), *pex6-2* stabilized ICL and MLS (Figure 6, E and F). The stabilization of ICL and MLS without dramatic effects on other peroxisomal processes such as matrix protein import (Figure 1E) suggests that ICL and MLS stabilization in *pex6-2* does not result from a failure to import ICL and MLS into the peroxisome, as in *pex14* alleles. Rather, it seems feasible that peroxisomal matrix proteins require the PEX5-recycling machinery, including PEX6 and PEX4, to move from the peroxisome to the cytosol for proteasomal degradation (Figure 8B).

Multiple genes contribute to efficient peroxisomal matrix protein degradation

By screening for mutants exhibiting GFP–ICL stabilization, we have begun identifying genes needed for matrix protein degradation and deciphering the peroxisome-associated

matrix protein degradation pathway (Figure 8B). We found that matrix proteins need to enter the peroxisome to be subject to efficient degradation and that the metabolic status of the peroxisome affects the degradation rate. Moreover, several peroxins involved in ubiquitinating and retrotranslocating PEX5 are needed for efficient degradation, consistent with the intriguing possibility that matrix proteins may leave the peroxisome for proteasomal degradation in the cytosol. The progress reported here also reveals several gaps in our understanding of peroxisome-associated matrix protein degradation that remain to be elucidated, including how matrix proteins are recognized for degradation and how metabolic status is linked to degradation rate. Several *pfl* mutants for which the defective genes have not been identified displayed neither IBA resistance nor sucrose dependence, but rather appeared to have wild-type β-oxidation phenotypes (Table 4). Identification of the genes defective in these mutants may provide additional insights into how peroxisomal proteins are degraded.

Acknowledgments

We thank John Harada (University of California, Davis) for the MLS antibody, Masayoshi Maeshima (Nagoya University, Japan) for the ICL antibody, Douglas Randall (University of Missouri, Columbia) for the HPR antibody, and Steven Smith and Itsara Pracharoenwattana (University of Western Australia) for the PMDH2 antibody. We are grateful to Wendell Fleming for assistance with confocal microscopy, Daniel Wagner for stereomicroscope use, Lucia Strader and Mauro Rinaldi for recombination mapping markers, and Emily Liljestrand for assistance in mapping *lon2-6*. We thank the *Arabidopsis* Biological Resource Center at Ohio State University for seeds from Salk Institute insertion lines and Lisa Farmer, Wendell Fleming, Kim Gonzalez, Yun-Ting Kao, and Mauro Rinaldi for critical comments on the manuscript. This research was supported by the National Institutes of Health (R01GM079177) and the Robert A. Welch Foundation (C-1309). Confocal microscopy was performed on equipment obtained through a Shared Instrumentation Grant from the National Institutes of Health (S10RR026399-01). M.J.L. was supported in part by a postdoctoral fellowship from the U.S. Department of Agriculture (2008-20659).

Literature Cited

Adham, A. R., B. K. Zolman, A. Millius, and B. Bartel, 2005 Mutations in *Arabidopsis* acyl-CoA oxidase genes reveal distinct and overlapping roles in β-oxidation. Plant J. 41: 859–874.

Azevedo, J. E., and W. Schliebs, 2006 Pex14p, more than just a docking protein. Biochim. Biophys. Acta 1763: 1574–1584.

Bartoszewska, M., C. Williams, A. Kikhney, L. Opalinski, C. W. Van Roermund *et al.*, 2012 Peroxisomal proteostasis involves a Lon family protein that functions as protease and chaperone. J. Biol. Chem. 287: 27380–27395.

Bell, C. J., and J. R. Ecker, 1994 Assignment of 30 microsatellite loci to the linkage map of *Arabidopsis*. Genomics 19: 137–144.

Boisson-Dernier, A., S. Frietsch, T.-H. Kim, M. B. Dizon, and J. I. Schroeder, 2008 The peroxin loss-of-function mutation *abstinence by mutual consent* disrupts recognition between male and female gametophytes. Curr. Biol. 18: 63–68.

Clough, S. J., and A. F. Bent, 1998 Floral dip: a simplified method for *Agrobacterium*-mediated transformation of *Arabidopsis thaliana*. Plant J. 16: 735–743.

Copenhaver, G. P., W. E. Browne, and D. Preuss, 1998 Assaying genome-wide recombination and centromere functions with Arabidopsis tetrads. Proc. Natl. Acad. Sci. USA 95: 247–252.

Cornah, J. E., V. Germain, J. L. Ward, M. H. Beale, and S. M. Smith, 2004 Lipid utilization, gluconeogenesis, and seedling growth in *Arabidopsis* mutants lacking the glyoxylate cycle enzyme malate synthase. J. Biol. Chem. 279: 42916–42923.

Davies, R. T., D. H. Goetz, J. Lasswell, M. N. Anderson, and B. Bartel, 1999 *IAR3* encodes an auxin conjugate hydrolase from Arabidopsis. Plant Cell 11: 365–376.

Eastmond, P. J., 2007 *MONODEHYROASCORBATE REDUCTASE4* is required for seed storage oil hydrolysis and postgerminative growth in Arabidopsis. Plant Cell 19: 1376–1387.

Eastmond, P. J., V. Germain, P. R. Lange, J. H. Bryce, S. M. Smith *et al.*, 2000a Postgerminative growth and lipid catabolism in oilseeds lacking the glyoxylate cycle. Proc. Natl. Acad. Sci. USA 97: 5669–5674.

Eastmond, P. J., M. Hooks, and I. A. Graham, 2000b The Arabidopsis acyl-CoA oxidase gene family. Biochem. Soc. Trans. 28: 95–99.

Fahnenstich, H., T. E. Scarpeci, E. M. Valle, U. I. Flugge, and V. G. Maurino, 2008 Generation of hydrogen peroxide in chloroplasts of Arabidopsis overexpressing glycolate oxidase as an inducible system to study oxidative stress. Plant Physiol. 148: 719–729.

Fujiki, Y., C. Nashiro, N. Miyata, S. Tamura, and K. Okumoto, 2012 New insights into dynamic and functional assembly of the AAA peroxins, Pex1p and Pex6p, and their membrane receptor Pex26p in shuttling of PTS1-receptor Pex5p during peroxisome biogenesis. Biochim. Biophys. Acta 1823: 145–149.

Gabaldon, T., B. Snel, F. Van Zimmeren, W. Hemrika, H. Tabak *et al.*, 2006 Origin and evolution of the peroxisomal proteome. Biol. Direct 1: 8.

Germain, V., E. L. Rylott, T. R. Larson, S. M. Sherson, N. Bechntold *et al.*, 2001 Requirement for 3-ketoacyl-CoA thiolase-2 in peroxisome development, fatty acid β-oxidation and breakdown of triacylglycerol in lipid bodies of *Arabidopsis* seedlings. Plant J. 28: 1–12.

Graham, I. A., 2008 Seed storage oil mobilization. Annu. Rev. Plant Biol. 59: 115–142.

Grimm, I., D. Saffian, H. W. Platta, and R. Erdmann, 2012 The AAA-type ATPases Pex1p and Pex6p and their role in peroxisomal matrix protein import in *Saccharomyces cerevisiae*. Biochim. Biophys. Acta 1823: 150–158.

Haughn, G. W., and C. Somerville, 1986 Sulfonylurea-resistant mutants of *Arabidopsis thaliana*. Mol. Gen. Genet. 204: 430–434.

Hayashi, M., K. Toriyama, M. Kondo, and M. Nishimura, 1998 2,4-Dichlorophenoxybutyric acid-resistant mutants of *Arabidopsis* have defects in glyoxysomal fatty acid β-oxidation. Plant Cell 10: 183–195.

Hayashi, M., K. Nito, K. Toriyama-Kato, M. Kondo, T. Yamaya *et al.*, 2000 *At*Pex14p maintains peroxisomal functions by determining protein targeting to three kinds of plant peroxisomes. EMBO J. 19: 5701–5710.

Hayashi, M., M. Yagi, K. Nito, T. Kamada, and M. Nishimura, 2005 Differential contribution of two peroxisomal protein receptors to the maintenance of peroxisomal functions in *Arabidopsis*. J. Biol. Chem. 280: 14829–14835.

Helm, M., C. Lück, J. Prestele, G. Hierl, P. F. Huesgen *et al.*, 2007 Dual specificities of the glyoxysomal/peroxisomal

processing protease DEG15 in higher plants. Proc. Natl. Acad. Sci. USA 104: 11501–11506.
Hoseki, J., R. Ushioda, and K. Nagata, 2010 Mechanism and components of endoplasmic reticulum-associated degradation. J. Biochem. 147: 19–25.
Hu, J., A. Baker, B. Bartel, N. Linka, R. T. Mullen *et al.*, 2012 Plant peroxisomes: biogenesis and function. Plant Cell 24: 2279–2303.
Keller, G. A., S. Gould, M. Deluca, and S. Subramani, 1987 Firefly luciferase is targeted to peroxisomes in mammalian cells. Proc. Natl. Acad. Sci. USA 84: 3264–3268.
Khan, B. R., and B. K. Zolman, 2010 pex5 Mutants that differentially disrupt PTS1 and PTS2 peroxisomal matrix protein import in Arabidopsis. Plant Physiol. 154: 1602–1615.
Kleczkowski, L. A., and D. D. Randall, 1988 Purification and characterization of a novel NADPH(NADH)-dependent hydroxypyruvate reductase from spinach leaves: comparison of immunological properties of leaf hydroxypyruvate reductases. Biochem. J. 250: 145–152.
Koller, A., W. B. Snyder, K. N. Faber, T. J. Wenzel, L. Rangell *et al.*, 1999 Pex22p of *Pichia pastoris*, essential for peroxisomal matrix protein import, anchors the ubiquitin-conjugating enzyme, Pex4p, on the peroxisomal membrane. J. Cell Biol. 146: 99–112.
Last, R. L., and G. R. Fink, 1988 Tryptophan-requiring mutants of the plant *Arabidopsis thaliana*. Science 240: 305–310.
Lazarow, P. B., 2006 The import receptor Pex7p and the PTS2 targeting sequence. Biochim. Biophys. Acta 1763: 1599–1604.
Leidhold, C., and W. Voos, 2007 Chaperones and proteases–guardians of protein integrity in eukaryotic organelles. Ann. N. Y. Acad. Sci. 1113: 72–86.
Li, F., and R. D. Vierstra, 2012 Autophagy: a multifaceted intracellular system for bulk and selective recycling. Trends Plant Sci. 17: 526–537.
Lingard, M. J., and B. Bartel, 2009 Arabidopsis LON2 is necessary for peroxisomal function and sustained matrix protein import. Plant Physiol. 151: 1354–1365.
Lingard, M. J., M. Monroe-Augustus, and B. Bartel, 2009 Peroxisome-associated matrix protein degradation in *Arabidopsis*. Proc. Natl. Acad. Sci. USA 106: 4561–4566.
Maeshima, M., H. Yokoi, and T. Asahi, 1988 Evidence for no proteolytic processing during transport of isocitrate lyase into glyoxysomes in castor bean endosperm. Plant Cell Physiol. 29: 381–384.
Manjithaya, R., T. Y. Nazarko, J. C. Farre, and S. Subramani, 2010 Molecular mechanism and physiological role of pexophagy. FEBS Lett. 584: 1367–1373.
Matsumura, T., H. Otera, and Y. Fujiki, 2000 Disruption of the interaction of the longer isoform of Pex5p, Pex5pL, with Pex7p abolishes peroxisome targeting signal type 2 protein import in mammals: study with a novel *PEX5*-impaired Chinese hamster ovary cell mutant. J. Biol. Chem. 275: 21715–21721.
Meinecke, M., C. Cizmowski, W. Schliebs, V. Kruger, S. Beck *et al.*, 2010 The peroxisomal importomer consitutes a large and highly dynamic pore. Nat. Cell Biol. 3: 273–277.
Michaels, S. D., and R. M. Amasino, 1998 A robust method for detecting single-nucleotide changes as polymorphic markers by PCR. Plant J. 14: 381–385.
Monroe-Augustus, M., N. M. Ramón, S. E. Ratzel, M. J. Lingard, S. E. Christensen *et al.*, 2011 Matrix proteins are inefficiently imported into Arabidopsis peroxisomes lacking the receptor-docking peroxin PEX14. Plant Mol. Biol. 77: 1–15.
Neff, M. M., J. D. Neff, J. Chory, and A. E. Pepper, 1998 dCAPS, a simple technique for the genetic analysis of single nucleotide polymorphisms: experimental applications in *Arabidopsis thaliana* genetics. Plant J. 14: 387–392.
Normanly, J., P. Grisafi, G. R. Fink, and B. Bartel, 1997 Arabidopsis mutants resistant to the auxin effects of indole-3-acetonitrile are defective in the nitrilase encoded by the *NIT1* gene. Plant Cell 9: 1781–1790.
Olsen, L. J., W. F. Ettinger, B. Damsz, K. Matsudaira, M. A. Webb *et al.*, 1993 Targeting of glyoxysomal proteins to peroxisomes in leaves and roots of a higher plant. Plant Cell 5: 941–952.
Ostersetzer, O., Y. Kato, Z. Adam, and W. Sakamoto, 2007 Multiple intracellular locations of Lon protease in Arabidopsis: evidence for the localization of AtLon4 to chloroplasts. Plant Cell Physiol. 48: 881–885.
Osumi, T., T. Tsukamoto, S. Hata, S. Yokota, S. Miura *et al.*, 1991 Amino-terminal presequence of the precursor of peroxisomal 3-ketoacyl-CoA thiolase is a cleavable signal peptide for peroxisomal targeting. Biochem. Biophys. Res. Commun. 181: 947–954.
Platta, H. W., F. El Magraoui, D. Schlee, S. Grunau, W. Girzalsky *et al.*, 2007 Ubiquitination of the peroxisomal import receptor Pex5p is required for its recycling. J. Cell Biol. 177: 197–204.
Platta, H. W., F. E. Magraoui, B. E. Baumer, D. Schlee, W. Girzalsky *et al.*, 2009 Pex2 and Pex12 function as protein-ubiquitin ligases in peroxisomal protein import. Mol. Cell. Biol. 29: 5505–5516.
Pracharoenwattana, I., J. E. Cornah, and S. M. Smith, 2007 *Arabidopsis* peroxisomal malate dehydrogenase functions in β-oxidation but not in the glyoxylate cycle. Plant J. 50: 381–390.
Ramón, N. M., and B. Bartel, 2010 Interdependence of the peroxisome-targeting receptors in *Arabidopsis thaliana*: PEX7 facilitates PEX5 accumulation and import of PTS1 cargo into peroxisomes. Mol. Cell. Biol. 21: 1263–1271.
Ratzel, S. E., M. J. Lingard, A. W. Woodward, and B. Bartel, 2011 Reducing PEX13 expression ameliorates physiological defects of late-acting peroxin mutants. Traffic 12: 121–134.
Reumann, S., C. Ma, S. Lemke, and L. Babujee, 2004 AraPerox. A database of putative Arabidopsis proteins from plant peroxisomes. Plant Physiol. 136: 2587–2608.
Reumann, S., L. Babujee, C. Ma, S. Wienkoop, T. Siemsen *et al.*, 2007 Proteome analysis of Arabidopsis leaf peroxisomes reveals novel targeting peptides, metabolic pathways, and defense mechanisms. Plant Cell 19: 3170–3193.
Schell-Steven, A., K. Stein, M. Amoros, C. Landgraf, R. Volkmer-Engert *et al.*, 2005 Identification of a novel, intraperoxisomal PEX14-binding site in PEX13: association of PEX13 with the docking complex is essential for peroxisomal matrix protein import. Mol. Cell. Biol. 25: 3007–3018.
Schluter, A., S. Fourcade, R. Ripp, J. L. Mandel, O. Poch *et al.*, 2006 The evolutionary origin of peroxisomes: an ER-peroxisome connection. Mol. Biol. Evol. 23: 838–845.
Schumann, H., P. F. Huesgen, C. Gietl, and I. Adamska, 2008 The DEG15 serine protease cleaves peroxisomal targeting signal 2-containing proteins in *Arabidopsis*. Plant J. 148: 1847–1856.
Stasinopoulos, T. C., and R. P. Hangarter, 1990 Preventing photochemistry in culture media by long-pass light filters alters growth of cultured tissues. Plant Physiol. 93: 1365–1369.
Strader, L. C., and B. Bartel, 2011 Transport and metabolism of the endogenous auxin precursor indole-3-butyric acid. Mol. Plant 4: 477–486.
Strader, L. C., M. Monroe-Augustus, and B. Bartel, 2008 The IBR5 phosphatase promotes Arabidopsis auxin responses through a novel mechanism distinct from TIR1-mediated repressor degradation. BMC Plant Biol. 8: 41.
Strader, L., A. Culler Hendrickson, J. Cohen, and B. Bartel, 2010 Conversion of endogenous indole-3-butyric acid to indole-3-acetic acid drives cell expansion in Arabidopsis seedlings. Plant Physiol. 153: 1577–1586.
Strader, L. C., D. L. Wheeler, S. E. Christensen, J. C. Berens, J. D. Cohen *et al.*, 2011 Multiple facets of Arabidopsis seedling development require indole-3-butyric acid-derived auxin. Plant Cell 23: 984–999.
Swinkels, B. W., S. J. Gould, A. G. Bodnar, R. A. Rachubinski, and S. Subramani, 1991 A novel, cleavable peroxisomal targeting sig-

nal at the amino-terminus of the rat 3-ketoacyl-CoA thiolase. EMBO J. 10: 3255–3262.

Thoms, S., and R. Erdmann, 2006 Peroxisomal matrix protein receptor ubiquitination and recycling. Biochim. Biophys. Acta 1763: 1620–1628.

Van Den Bosch, H., R. B. Schutgens, R. J. Wanders, and J. M. Tager, 1992 Biochemistry of peroxisomes. Annu. Rev. Biochem. 61: 157–197.

Wanders, R. J. A., and H. R. Waterham, 2005 Peroxisomal disorders I: biochemistry and genetics of peroxisome biogenesis disorders. Clin. Genet. 67: 107–133.

Willekens, H., S. Chamnongpol, M. Davey, M. Schraudner, C. Langebartels *et al.*, 1997 Catalase is a sink for H2O2 and is indispensable for stress defence in C3 plants. EMBO J. 16: 4806–4816.

Williams, C., and B. Distel, 2006 Pex13p: Docking or cargo handling protein? Biochim. Biophys. Acta 1763: 1585–1591.

Woodward, A. W., and B. Bartel, 2005 The *Arabidopsis* peroxisomal targeting signal type 2 receptor PEX7 is necessary for peroxisome function and dependent on PEX5. Mol. Biol. Cell 16: 573–583.

Zolman, B. K., and B. Bartel, 2004 An Arabidopsis indole-3-butyric acid-response mutant defective in PEROXIN6, an apparent ATPase implicated in peroxisomal function. Proc. Natl. Acad. Sci. USA 101: 1786–1791.

Zolman, B. K., A. Yoder, and B. Bartel, 2000 Genetic analysis of indole-3-butyric acid responses in *Arabidopsis thaliana* reveals four mutant classes. Genetics 156: 1323–1337.

Zolman, B. K., I. D. Silva, and B. Bartel, 2001 The Arabidopsis *pxa1* mutant is defective in an ATP-binding cassette transporter-like protein required for peroxisomal fatty acid β-oxidation. Plant Physiol. 127: 1266–1278.

Zolman, B. K., M. Monroe-Augustus, I. D. Silva, and B. Bartel, 2005 Identification and functional characterization of *Arabidopsis* PEROXIN4 and the interacting protein PEROXIN22. Plant Cell 17: 3422–3435.

Zolman, B. K., M. Nyberg, and B. Bartel, 2007 IBR3, a novel peroxisomal acyl-CoA dehydrogenase-like protein required for indole-3-butyric acid response. Plant Mol. Biol. 64: 59–72.

Zolman, B. K., N. Martinez, A. Millius, A. R. Adham, and B. Bartel, 2008 Identification and characterization of *Arabidopsis* indole-3-butyric acid response mutants defective in novel peroxisomal enzymes. Genetics 180: 237–251.

Communicating editor: S. Poethig